Dalila Augusta Ferreira Mendes Lopes

Licenciada em Ciências da Engenharia Biomédica

Molecular Imprinting as a tool for producing Molecularly Intelligent Scaffolds for Tissue Engineering

Dissertação para obtenção do Grau de Mestre em
Engenharia Biomédica

Orientadores: Doutor Pedro Lopes Granja, Professor Afiliado, ICBAS, Professor Auxiliar Convidado, FEUP, Coordenador Adjunto do Programa Host Interaction and Response, i3S
Doutora Maria Goreti Ferreira Sales, Professora Adjunta, ISEP

Co-orientadora: Doutora Aureliana Filipa Sousa, Investigadora Assistente, i3S

Júri:

Presidente: Doutora Célia Maria Reis Henriques
Arguente: Doutora Teresa Maria Alves Casimiro Ribeiro
Vogais: Doutora Teresa Maria Alves Casimiro Ribeiro
Doutora Maria Goreti Ferreira Sales

FACULDADE DE
CIÊNCIAS E TECNOLOGIA
UNIVERSIDADE NOVA DE LISBOA

Novembro, 2017

Molecular Imprinting as a tool for producing Molecularly Intelligent Scaffolds for Tissue Engineering

"I am no longer accepting the things I cannot change,
I am changing the things I cannot accept."

Angela Davis, Academic and political activist

Agradecimentos

Quando se está prestes a chegar ao fim de uma etapa, é importante agradecer àqueles que fizeram parte dela e que contribuíram para o seu progresso. As palavras podem não ser suficientes, mas são sentidas.

Em primeiro lugar, gostaria de agradecer ao Professor Pedro Granja por tudo. Por me ter acolhido no grupo, por ter sempre depositado confiança em mim, por ter sempre um sorriso, otimismo e a capacidade de tornar fácil qualquer situação que pudesse parecer impossível de resolver, no momento. Tenho de agradecer por tê-lo conhecido, pois tornou-se uma inspiração para mim, pelo profissionalismo e pela paixão pela investigação! Muita força!

Em segundo lugar, à Professora Goreti Sales, pela total disponibilidade e ajuda durante este percurso, pelo espírito motivador e pela confiança, principalmente quando me motivou para participar no GSS-MIP. Foi um momento aterrador, no início, mas que me permitiu evoluir e por isso só posso agradecer a oportunidade!

Em terceiro lugar, à Professora Filipa Sousa, pela confiança que depositou em mim, pela orientação no projeto e pela boa-disposição!

E agora, um especial agradecimento à Mariana Neves. Primeiro, por ter "desbravado" um tema ainda assim pouco explorado. Segundo, por ter estado sempre pronta a ajudar-me, ouvir-me e orientar-me. Terceiro, por me incentivar, mesmo sem saber, para fazer um bom trabalho. Foste incrível, sem a tua ajuda, este trabalho não seria o que é hoje. Muito obrigada por tudo!

Também gostaria de agradecer a todos os que fazem e os que fizeram parte do fantástico grupo BioCarrier! Gostaria de agradecer ao Marco Araújo, Rúben Pereira e Sara Neves, pela orientação e ajuda em algumas fases do trabalho.

Não posso deixar de agradecer ao Manuel de Barros, Carolina Paredes, Carlos Diogo, Adele Cook, Daniel Carvalho, Ana Nascimento, Juliana Dias e Miguel Ferreira, pela amizade, pelos momentos de convívio e pelas risadas. Estes momentos vão deixar-me sempre com um sorriso no rosto.

Um grande "Havla!" à Tanja Cernosa, pelo carinho e motivação, apesar da distância.

Um grande obrigado às minhas meninas da margem sul, Daniela Medley e Jéssica Costa, por todos os bons momentos que passámos ao longo destes seis anos, pelas aventuras e pela grande amizade que temos.

Não posso esquecer de agradecer àqueles amigos de infância, que embora não estejam sempre perto fisicamente, estão sempre perto no coração e em todos os momentos. Gostaria de agradecer à Patrícia Azevedo, Sofia Valente, Pedro Ribeiro, Sofia Gonçalves e Diogo Monteiro. Só tenho a agradecer as conversas, os conselhos, o carinho, o apoio e a motivação nos momentos mais cinzentos. Sem vocês, a jornada não teria sido tão feliz!

Um enorme agradecimento à minha família! À minha irmã Diana, por sempre ter colocado a fasquia alta e me motivar para ser melhor no meu trabalho e nas minhas escolhas. À minha irmã Dáldia, por me motivar a ser um exemplo e uma irmã melhor. E, principalmente, aos meus pais, João e Maria Augusta, pelos sacrifícios que fizeram e ainda fazem, e por me

ensinarem que o esforço compensa. E um especial agradecimento ao recente membro da família, a minha sobrinha Aleena Umo-Culsum, por de forma tão simples, me fazer ver o mundo de outra forma e me motivar para, no futuro, ser um modelo a seguir no decorrer da vida dela!

Obrigada por tudo!

Abstract

Tissue Engineering creates strategies capable of interacting with cells, to promote tissue regeneration. Cell adhesion is essential in cell communication and regulation, and cell-scaffold interactions occurring at the surface of the material are dependent on the biomolecules adsorbed. This knowledge promotes the biofunctionalization of biomaterials to enhance cellular response. Molecular Imprinting (MI) is an alternative to molecular recognition phenomena present in living systems, such as the antibody-antigen bonding, and has been proposed as a biofunctionalization method to improve scaffolds selectivity and recognition. The principle of MI is the polymerization of monomers and crosslinkers in the presence of the template molecule of interest and the subsequent removal of the template. The crosslinker enables the formation of specific cavities, which enables the material to recognize the template. The challenging in MI is the incorporation of biomacromolecules important for the wound healing. The imprinting of biomacromolecules holds drawbacks associated to the high molecular weight and complex structure.

This work proposes a MI system based on methacrylated alginate imprinted with the model protein bovine serum albumin (BSA), using photo-polymerization. A non-imprinted polymer acting as control was also prepared by photo-polymerization without BSA. The effect of two crosslinkers and a monomer on mechanical properties of polymer discs was studied and the results revealed an improvement of the mechanical properties of crosslinked polymers. The template removal and rebinding capacity were also characterized for molecularly imprinted discs. The template removal showed results below 70%, most likely due to the amount of methacrylated alginate (4% w/v) and the bulk imprinting. Results concerning the capacity of the molecularly imprinted material to recognize BSA showed higher results when comparing to non-imprinted polymers. However, the system still needs to be improved, concerning the template removal and rebinding capacity. Still, it enabled the understanding of the effect of different crosslinkers on MI.

Keywords: Tissue engineering, molecular imprinting, bulk imprinting, molecularly imprinted scaffold, methacrylated alginate, crosslinker.

Resumo

A engenharia de tecidos cria estratégias capazes de interagir com células, para promover a regeneração de tecidos. A adesão celular é essencial na comunicação e na regulação, e a interação entre células e matriz, na superfície do material, é dependente das biomoléculas adsorvidas. Este conhecimento sustenta a necessidade de biofuncionalização de biomateriais para melhorar a resposta celular. A Impressão Molecular (MI, do inglês, *Molecular Imprinting*) é uma alternativa aos fenómenos de reconhecimento molecular presentes em sistemas vivos, como a ligação anticorpo-antigénio, e tem sido proposta para biofuncionalização, melhorando seletividade e reconhecimento das matrizes. Em MI, ocorre polimerização de monómeros e reticulante na presença da molécula a imprimir e subsequente remoção. A presença do reticulante permite a formação de cavidades específicas, tornando o material capaz de reconhecer a molécula. O desafiante na MI é a incorporação de biomacromoléculas envolvidas no processo de cicatrização. A MI de biomacromoléculas possui desvantagens associadas ao elevado peso molecular e estrutura complexa.

Este trabalho propõe um sistema baseado em alginato metacrilado impresso com a proteína modelo albumina de soro bovino (BSA), utilizando foto-polimerização. Um polímero não impresso que atua como controlo foi também preparado por foto-polimerização, sem BSA. Foi estudado o papel de dois agentes de reticulação e de um monómero, nas propriedades mecânicas dos discos, obtendo-se melhores propriedades mecânicas em polímeros reticulados. A capacidade de remoção e adsorção também foi caracterizada para discos impressos. A remoção de BSA mostrou um resultado abaixo de 70%, provavelmente devido à concentração de alginato metacrilado (4% w/v) e à impressão em *bulk*. A capacidade do material impresso em reconhecer BSA foi superior, comparando ao material não impresso. Embora o sistema precise de ser melhorado, quanto à remoção da proteína e à eficiência da adsorção, ele permitiu a compreensão do efeito de diferentes agentes de reticulação no processo.

Palavras-chave: Engenharia de tecidos, impressão molecular, impressão em *bulk*, matriz molecularmente impressa, alginato metacrilado, agente reticulante.

Table of contents

List of Figures

List of Tables

xx

List of Abbreviations

AAm – Acrylamide

AL - Alginate

ALMA – Methacrylated alginate

APS – Ammonium persulfate

AU – Arbitrary Units

bFGF – Basic Fibroblast Growth Factor

BSA – Bovine serum albumin

Cryo-SEM – Cryo Scanning Electron Microscopy

DEAEM – 2-(Ethylamino)ethyl methacrylate

DI water – Deionized water

DM – Degree of methacrylation

DMEM – Dulbecco's Modified Eagle's Medium

ECM – Extracellular matrix

EGDMA – Ethylene glycol dimethacrylate

Fn – Fibronectin

Hb – Hemoglobin

^{1}H NMR – Proton Nuclear Magnetic Resonance

IF – Imprinting factor

Irg – Irgacure 2959

LVR – Linear viscoelastic region

MA – Methacrylate Anhydride

MBAAm – N,N′-methylenebis(acrylamide)

MI – Molecular Imprinting

MIP – Molecularly imprinted polymer

NI – Non-imprinted

NIP – Non-imprinted polymer

pI – Isoelectric point

PBS – Phosphate buffered saline

PEG – Poly(ethylene glycol)

PEGDA – Poly(ethylene glycol) diacrylate

PLGA – Poly(glycolic acid)

PVA – Polyvinyl alcohol

Q – Rebinding capacity

RGD – Arginine-glycine-aspartic acid

RT – Room Temperature

SEM – Standard Error of Mean

SR – Swelling Ratio

TBS – Tris(hydroxymethyl)aminomethane buffered saline

TE – Tissue Engineering

TGF-β – Transforming growth factor β

Tris – Tris(hydroxymethyl)aminomethane

UV – Ultraviolet

Chapter 1 - General Introduction

Along the time, there have been important discoveries made on science that rapidly changed and improved medical practice, with the goal of enhancing life expectancy. This improvement on longevity has been representing some challenges concerning life quality and resolution to diseases.

With the aim to solve some of the concerns of the society of today, we are witnessing great improvements on the biomedical field. The multidisciplinary field of Tissue Engineering (TE) is one of the great promises. This field aims for the replacement, treatment or recovery of damaged or diseased organs and tissues functions. To understand how TE can accomplish those aims, it is important to understand how an injury can trigger a cascade of events and how the strategies TE adopts can be adapted to enhance the tissue healing capacities.

1.1. Wound Healing

Immediately after a tissue injury, the human body's natural response is the activation of the wound healing process or the so called wound healing cascade. Wound healing is divided into three phases that occur in parallel with homeostasis: inflammation, tissue formation and tissue remodelling [1].

The first step is not the repair of the damaged tissue, but the stop of the blood flow from the wound. At the injury site, an aggregation of thrombocytes leads to the formation of a fibrin clot to prevent excessive blood loss. Cells trapped in the clot release growth factors, which lead to an inflammatory process where monocytes-macrophages, lymphocytes, fibroblasts and endothelial cells are chemo-attracted to the site, represented on the right side of **Figure 1.1**. The different growth factors and cytokines produced by the macrophages will promote the formation of a new connective tissue, granulation tissue, which provides a vascularized network for the deposition of collagen, and stimulate fibroblast migration, proliferation and angiogenesis (formation of newly microscopic blood vessels) [2]. At this stage, fibroblasts will grow and form a new Extracellular matrix (ECM) by excreting collagen and fibronectin [1]. The wound contraction that happens next is mediated by endothelial cells which revascularize the damaged region. Fibroblasts differentiate into myofibroblasts and contract the matrix to bring together the edges of the wound [3]. Finally, at the maturation and remodelling phase, collagen is remodelled and realigned along tension lines [1].

As a result of injury, the tissue can respond by either creating a scar or achieving full regeneration. The tissue or organ may be able to fully recover structure, composition and function, or the wound healing cascade and the increased tissue tension can be responsible for the formation of scar, and the result in humans is often fibrous tissue deposition at the expense of tissue regeneration [1]. For not deep injuries, this means small and superficial wounds, the wound healing process leads to regeneration rather than to the formation of a scar. On the other hand, fully regeneration can be achieved at embryonic stages, since fetal skin has the ability to not forming scar due to differential expression and production of collagen and Hyaluronic Acid

(HA), among other elements, present on the ECM [4]. The ideal biomaterial or scaffold system should enhance tissue regeneration and decrease scar formation [1] and that is TE main goal.

The final outcome of tissue repair strongly depends on the duration and intensity of each wound healing stage. Even though inflammation is a prerequisite for tissue regeneration, unresolved chronic inflammation at a wound site may favour scarring processes, excessive fibrosis and non-healing wounds [3], thus, critically affecting TE strategies.
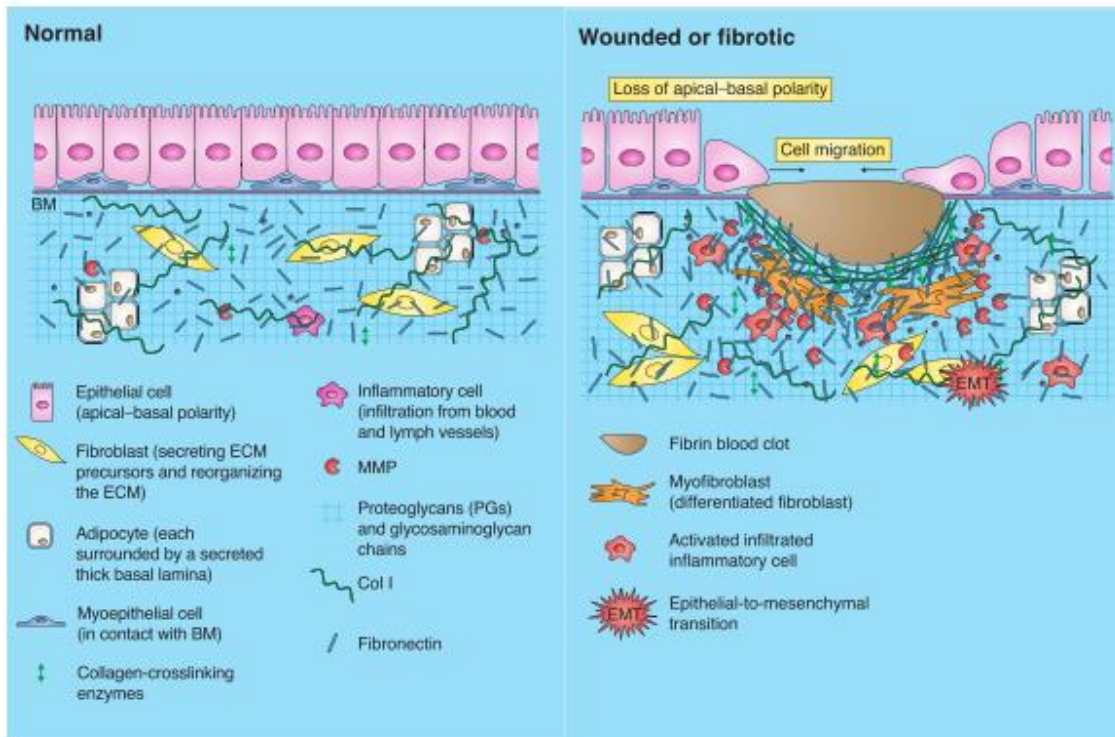
Figure 1.1. Differences on the structure and the components present, between normal and wounded ECM. There is an increase on the stiffness of the wounded and fibrotic ECM. **Adapted from** [5]

1.2. Tissue Engineering

So the tissue can accomplish full or partial regeneration, TE applies biocompatible materials, so called biomaterials, and/or different strategies to achieve tissue regeneration.

Regenerative medicine is based on cell biology with the aim to generate viable cells, tissues or organs with biological functions for specific therapeutic applications. In this context, the cell therapies are particularly based on stem cells [6], [7], to develop new tissue and improve the cell-based TE approaches. The four major approaches used are local targeting of connective tissue progenitors, transplantation of autogenous connective tissue, transplantation of culture-expanded or modified connective tissue and transplantation of fully formed tissue [8].

Biophysical stimulation is used for cell targeting, and it is based on *in vivo* electricity caused by cells, due to the presence of ion channels within the cell membranes [9]. The

approaches include electrical stimulation [10], [11], to promote cellular growth, differentiation and possible healing. This field has been proven to potentially facilitate stem cell differentiation, cell integration into the environment and control of cell distribution patterns induced by directional electromigration [11].

Both cell-therapy and electrical stimulation approaches have the potential to control the cell behaviour and incorporation into engineered materials, leading to a more effective regenerative medicine.

The other approach largely described on literature involves the use of biomaterials. These materials should biomimic and modulate the natural events concerning the wound healing process, in a way to optimize tissue regeneration. Scaffold-based approaches rely on the structural support provided by these materials for cell attachment and proliferation, and the subsequent development of new tissue. The scaffolds and matrices produced with these biomaterials work as temporary tissues that support cell adhesion while the primary tissue is not yet repaired. Three-dimensional scaffolds with architectural and specific mechanical features for clinical applications and chemically modified surfaces with biologically active molecules (adhesion sites, growth factors or peptides) [12], [13] can improve cell attachment, migration and differentiation. The ideal is that these structures provide a void volume to promote vascularization, which influences the new tissue formation [8]. The design of biomimetic materials aims to create materials capable of specific interactions with cells from the surrounding tissues by promoting a scaffold-ECM interaction [13].

1.3. Extracellular Matrix

ECM is a dynamic network of fibrous adhesion proteins, proteoglycans and water. It is a non-cellular component, present within all tissues and organs, and provides physical scaffolding for the cellular constituents. It is the ECM that initiates important biochemical and biomechanical processes that are required for tissue morphogenesis, differentiation and homeostasis. Each tissue has an ECM with a unique composition and topology.

ECM is composed of two main classes of macromolecules: proteoglycans and fibrous proteins. These molecules are strictly organized and the organization determines the bioactivity of the ECM [14]. ECM can also act as a provisional matrix for growth factors and other proteins, upon wounding [2].

The proteoglycans include glycosaminoglycans, which are linear unbranched polymers of repeating disaccharides covalently linked to core proteins to form proteoglycans [15].

The main fibrous structural proteins are collagens, elastin, fibronectin (Fn), laminin and tenascin. Collagens, which constitute the main structural element of ECM, provide tensile strength and cohesiveness to tissues and contributes for the physical properties of their ECMs [15], [16]. The elastin fibers are covered by glycoprotein microfibrils, mainly fibrillins. Fn is an important macromolecule of ECM and it is an adhesive glycoprotein, involved in mediating cell attachment and function, and binding to growth factors [5], [17]. Fn also regulates the composition and stability of the ECM and is an important regulator of the formation and stability of cell–matrix fibrillar adhesions [18].

During wound healing, ECM suffers changes, namely on the structure, molecular composition, and biological and mechanical properties (**Figure 1.1**). Interactions among the ECM, growth factors and cells are on the basis of tissue formation and regeneration, including wound healing. The whole process of wound healing, described previously, leads to an increase of mechanical stress and stiffness caused by the synthesis of large quantities of ECM proteins, including collagen type I and III, Fn and HA [5], which contribute for the structural integrity of the matrix during the stages of tissue repair. During wound healing, there is an increase of these proteins and fibrin, as well. These create a provisional matrix to promote cell migration and adhesion, but once the new tissue begins to form, its appearance is restricted to the basement membrane zone of the dermal–epidermal junction and of the blood vessels [2].

ECM can be remodelled in response to signals from ECM receptors, such as integrins, laminin receptors or ECM-modifying proteins, such as matrix metalloproteinases, and also by extracellular and cellular tension [19].

Growth factors also regulate the ECM by stimulating cells to increase the production of ECM components or enhance synthesis of matrix metalloproteinases, enzymes that degrade ECM to allow cell growth and to improve remodelling [20]. ECM can bind to and release certain important growth factors, during wound healing stages. One example is the case of the binding of basic fibroblast growth factor (bFGF) to heparan sulfate [21], a proteoglycan present in ECM. This growth factor is important on promoting fibroblasts proliferation, neovascularization and increasing the synthesis of collagenase. The properties of this growth factor were studied by S. Matsumoto *et al.* [22] on a bFGF-impregnated gelatin sheet. This group performed studies concerning wound closure and morphological features, to prove that wounded animals treated with bFGF-impregnated gelatin sheet showed a faster wound closure, an increase on collagen maturity and enhancement of wound vascularization. Overall, this group seemed to prove the importance of this growth factor on promoting wound healing. Another important growth factor is the transforming growth factor-β (TGF-β) related to the expression of collagen and Fn into the ECM [23].

It is clear that ECM and its components affect wound healing fate, so TE must look for approaches that serve as guidance during the process of healing and that can incorporate both ECM and growth factors.

1.4. Design of scaffolds

Considering the major role of ECM in wound healing, a scaffold should be designed to resemble the functions of ECM and mimic its physiological conditions. For this purpose, a wide range of parameters should be considered, namely: type of material source (natural, polymeric or hybrid), porosity, surface chemistry, the responses to the surrounding environment (behaviour to pH or degradation characteristics), mechanical properties and the cellular response triggered by the material.

Scaffolds can be made from many biomaterials, but the more investigated are the polymeric ones, such as the biological polymers collagen, HA or alginate, due to their biodegradability [24]–[27]. Synthetic polymeric biomaterials like poly-L-lactic acid (PLLA), poly-glycolic acid (PGA) or poly-lactic-co-glycolic acid (PLGA) are applied as scaffolds, as well [28],

[29], but they may present some reduced bioactivity, which in turn can be further improved by the incorporation of growth factors or important ECM proteins on the scaffold [30].

Other materials chosen to design scaffolds comprise tissue-derived (allograft bone matrix) [31], ceramics or mineral-based [32] and composites [33] which are biocompatible and characterized by high mechanical stiffness and low elasticity, more indicated to hard tissues such as on orthopedic applications and combination with metals (titanium, for example) [34].

Considering that a scaffold should be porous to enable vascularization and host tissue integration upon implantation [35], allowing effective nutrient supply, gas diffusion and metabolic waste removal, most methods for fabricating porous scaffolds involve gas-based approaches: gas foaming or emulsion templating [36], [37], particle or solvent leaching [36], freeze-drying [38], [39] and electrospinning [6] to create distributed voids and connecting pores. Particularly in the gas foaming technique, a foaming agent such as sodium bicarbonate is added into the polymer phase to generate an inert gas such as N_2 or CO_2 at moderate acidic solutions [36] and the porous structure of the polymer is then formed, as soon as the dispersed gas phase is removed from the continuous phase of the polymer. Porosity and pore interconnectivity are essential aspects of scaffolds for TE. The existence of pores regulates the mass transfer and has a great impact on the cell adhesion and penetration into the scaffolds to form a new tissue. If pores are too small, there will be a limited diffusion of nutrients and removal of waste products. On the other hand, if pores are too large there will be a decrease in the specific surface area available, which limits cell attachment. The importance of a porous structure on promoting angiogenesis was studied by T. Tokatlian *et al.* [26]. The group studied the hypothesis of the rate and maturity of infiltrating vessels being enhanced by complementing the open pore structure with the delivery of DNA encoding for angiogenic growth factors. They studied two porous and non-porous HA hydrogels loaded with pro-angiogenic or reporter plasmid nanoparticles of 100 and 60 µm and they concluded that the pore size seemed to be the dominant factor in determining the angiogenic response to the hydrogels, with 60 µm porous hydrogels having more vessels present per area than the ones with 100 µm at the initial onset of angiogenesis at 3 weeks.

Biocompatibility is another fundamental feature to promote cell adhesion, proliferation and migration, so the tissues surrounded do not suffer a severe inflammation and the biomaterial is not rejected. The scaffolds should be biodegradable and the degradation products released over time into the site injury should be nontoxic and inoffensive to the surrounding tissues and organs, so the material can be replaced by natural ECM.

At the time the scaffold is implanted, the interaction between the environment and the biomaterial occurs through macromolecules, which adsorb at the surface of the biomaterial, triggering events that are responsible for mediating the cellular response.

Integrins mediate cellular interactions with biomaterials by binding to adhesive extracellular ligands that can be adsorbed from blood, plasma, or serum, secreted and deposited onto the biomaterial surface by cells, such as Fn and collagen, and/or bio-adhesive motifs, such as Arginine-glycine-aspartic acid (RGD) sequence, engineered at the biomaterial [40]. The Vroman effect explains the phenomena of protein adsorption into the surfaces of the biomaterials. The protein layer at the interface changes over time, due to proteins with higher concentration being adsorbed first, but are subsequently displaced by proteins that have higher affinity for the surface of the biomaterial. The proteins adsorbed mediate the interaction of the material to the cells.

Cell adhesion is essential in cell communication and regulation, therefore being crucial in the development and maintenance of tissues. It is already present that the cell-scaffold interaction is mediated through events occurring at the surface of the material, where proteins adsorbed influence the type of downstream events occurring upon cell binding. Thus, cell adhesion is affected by surface hydrophilicity, charge density and by the presence of specific chemical groups [41], [42]. This knowledge promoted the development of biofunctionalization techniques that enhances the interaction between cells and biomaterials.

Biological modifications can enhance cell attachment by incorporating cell recognition sites into the material, such as immobilization of biomolecules, natural ECM proteins (Fn and collagen) [24], [43], peptide sequences [12], [44], [45] or growth factors [22]. Peptides sequences have some advantages over whole proteins, related to the ability of the peptides to not fold, differently from proteins, which allows the receptor binding domains to remain available.

RGD is a sequence naturally existing in the ECM and is one of the most prominent structures for cell adhesion and cellular spreading. RGD sequence resides within a hydrophilic loop of either Fn, vitronectin, tenascin and other ECM proteins [15]. The cell surface receptors on the ECM, called integrins, recognize the RGD sequence of various proteins, such as Fn, fibrinogen, laminin, entactin, tenascin, osteopontin, and collagens [46], turning RGD into a molecule with a significant role in the recognition system of cell adhesion. Diverse works have been developed using RGD into the scaffold to promote cell-matrix adhesion and cellular response and viability. S. C. Neves *et al.* [12] biofunctionalized pectin hydrogels with a RGD-containing peptide and they were successful on showing that the cells within the matrices with RGD were able to spread and establish contact with each other, leading to the recreation of an intercellular network or a microtissue. S. G. Guerreiro *et al.* [47] also used RGD, but in this case grafted in fibroblasts immobilized alginate gels to study the recruitment of endothelial cells to improve vascularization. This group used different angiogenesis assays to test the influence of fibroblasts in the vascularization process and they came to the conclusion that fibroblasts immobilized within RGD-alginate gels were capable of influencing the formation of capillary-like structures by neighbouring endothelial cells.

1.5. Molecular Imprinting

Innovative functionalization strategies are gaining increasing interest in research and TE. Molecular Imprinting (MI) technology is an alternative to molecular recognition features present in biological systems, such as those activated by antibodies or even enzymes and biological receptors. This technology has been proposed as a different biofunctionalization method to improve scaffolds bioactivity [48] by mimicking the molecular recognition phenomena present in living systems.

The aim of this technology is to confer recognition and molecular memory to a material, which means that a molecule may be selectively recognized by that material, being preferred against other molecules. The design of a macromolecular chemical architecture that can recognize target molecules from an ensemble of closely related molecules enables the creation of materials with specificity and selectivity over the target molecule.

Until now, the most extensively studied applications of MI are mainly in the field of affinity chromatography [49] and (bio)sensor technology [50]–[52]. However, MI may prove itself to be a versatile technology to produce scaffolds for TE applications due to the wide range of monomers that can be used, type and degree of crosslinking, and strategies used to remove the template. MI is also characterized by the simplicity of use, the relatively low cost and the broad range of possible template molecules with biological interest (small organic molecules, ions and also biomacromolecules).

1.5.1. Main features

The principle of the technology is the polymerization of one or two monomers in the presence of the target molecule (template) which is incorporated into the material matrix.

The overall process is represented in **Figure 1.2** and starts with the dissolution of the template, functional monomers, including or not a crosslinking agent, and a polymerization initiator, such as radical initiators (ammonium persulfate (APS), benzoyl peroxide and others) that can induce chemical, electrical or photoinitiation [49], [50], [53]–[55]. The formation of a stable template-monomer complex during the pre-polymerization is a prerequisite for the success of MI and it allows the template position to be imprinted, with the help of crosslinking monomers. The final result is a polymer with affinity towards the template, either by its available binding sites or cavity shaped and size.

Since the aim of MI is to detect and recognize the template molecule, after polymerization, the template is removed by washing procedures with proper solvents. Unreacted monomers and crosslinkers are also removed in these steps. Template removal can be performed by using organic or inorganic solvents [53], [56], [57] or enzymatic digestion [58].
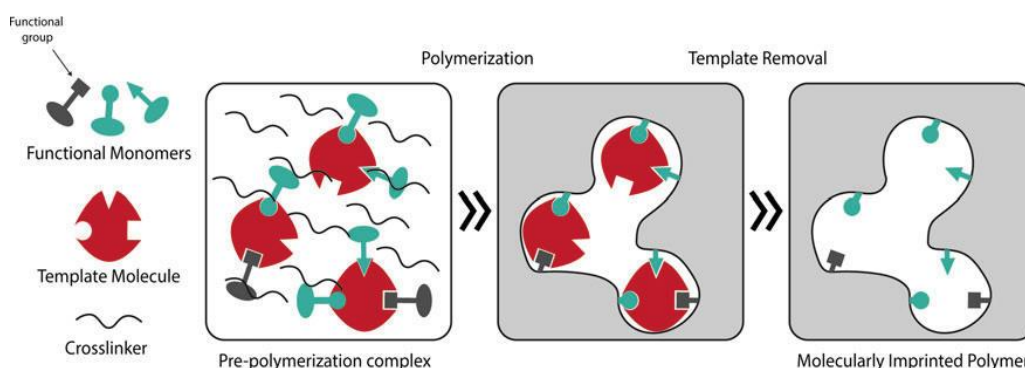
Figure 1.2. Outline of MI, involving the polymerization of functional monomers, the template molecule and possible crosslinkers. **From** [48]

After the imprinting process is completed, the imprinting efficiency can be evaluated by two main parameters [59]: adsorption capacity (Q, µg mg^{-1}) (**Equation 1**), which determines the amount of adsorbed molecules per weight of polymer; and imprinting efficiency or imprinting factor (IF) (**Equation 2**), which corresponds to the ratio between both molecularly-imprinted polymer (MIP) and corresponding non-imprinted polymer (NIP) adsorption capacities.

$$Q = \frac{(C_i - C_f)V}{W} \tag{1}$$

$$IF = \frac{Q_{MIP}}{Q_{NIP}} \tag{2}$$

In these, C_i and C_f are the initial and final concentration of template solution, respectively (µg mL^{-1}), V is the volume of the template solution (mL), W is the weight of MIP or NIP (mg) and Q_{MIP} and Q_{NIP} are the adsorption capacities of the MIP and NIP, respectively.

The interactions between monomer and template during polymerization of the molecularly imprinted material represent an essential condition to obtain networks with potential recognition sites [60]. Several strategies differ on the approach adopted to assemble the material, which are summarily described on the next section.

The choice of the template depends on the aim of the research, but diverse molecules have been used, such as proteins [56], [59], [61], drugs [50] and metal ions [62].

1.5.2. Imprinting strategies

There are different strategies to imprint a given template, which are illustrated in **Figure 1.3**.
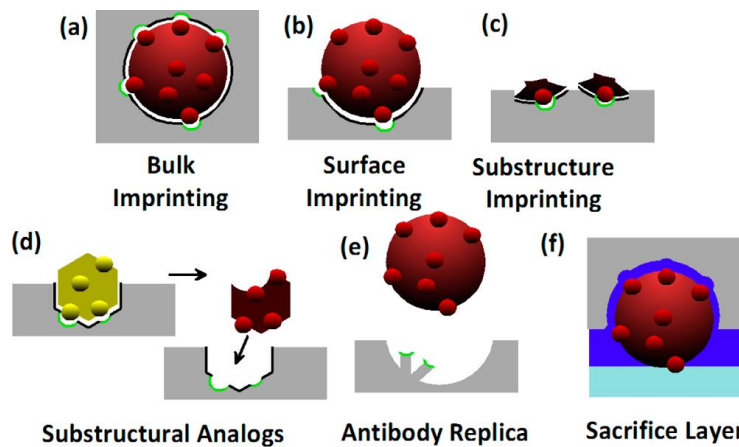
Figure 1.3. Several approaches for the development of MI materials. **From** [63]

In bulk imprinting (**Figure 1.3.a**), when a template molecule is added to the pre-polymer, the selective cavities are distributed all over the bulk, inside the inner layers of the polymer. This approach may represent an issue to complete template removal, since the templates with large sizes are more difficultly removed.

The surface imprinting (**Figure 1.3.b**) involves only the imprinting at the surface of a material. Surface imprinting [62] has been the aim of many researchers, due to the easier removal of the template molecule, comparing to bulk imprinting.

Substructure imprinting or epitope imprinting (**Figure 1.3.c**) is an alternative that does not involve the whole macromolecule as a template, but only relevant domains (epitopes) are used in the process and the polymer can recognize the entire protein [52], [53]. These fragments are located in the receptor domains or in other parts directly involved in the molecular recognition process.

The rest of the methods illustrated (**Figure 1.3.d-f**) consist in not using the template directly. The method of antibody replica was performed by R. Schirhagl *et al.* [64], who developed a polymer templated with immunoglobulins, and then used these MIP as stencils for designing actual plastic replicas of the initial antibody. The group found that molecular recognition based on noncovalent binding, such as hydrogen bonds or hydrophobic interactions, occurs and it is an expected behaviour for immune recognition, which usually takes place at a defined receptor site of the respective antigen. The resulting imprinted materials clearly reproduced the shape of the human immunoglobulin and the details of the specific binding sites on a molecular level. The method of sacrifice layer was studied by R. Agarwal *et al.* [54], who decided to address the challenges in top-down fabrication of nanocarriers, developing a biopolymer-based sacrificial release layer in combination with an improved nanocarrier-material. They concluded that the sacrificial layer improved scalability and ease of imprint-surface modification due to its switchable solubility through simple ion exchange between monovalent and divalent cations. This process can perform large-scale and efficient bio-nanoimprinting.

For TE applications, biological macromolecules are important templates due to their role in the healing process. However, proteins present many potential recognition sites with complex structures and conformation highly sensitive to pH, ionic strength and temperature. The preparation of effective imprints for macromolecule templates (Molecular weight > 1500 Da) [65] brings additional challenges, when compared to smaller molecules, due to their size, chemical structure and conformational fragility. The conditions in which the imprinting is performed must be mild to avoid protein denaturation during the polymerization, in order to not compromise the imprinting features. A major challenge is the solvent used to mixture all the MI components, which should not interfere with the monomer-template interaction while still allowing the complete miscibility between the components. Despite of proteins being completely miscible in aqueous solutions, water can disrupt hydrogen bonding between the monomer and template, one of the interactions systems rely for recognition [65].

Most of the protein MIP studies are developed for model macromolecules like lysozyme [58], bovine serum albumin (BSA) [59] and hemoglobin (Hb) [61], [66] but the forward aim is to develop systems recognizing more important biomacromolecules.

Fn is a high molecular weight (two polypeptides of molecular ~220 kDa each) with much potential to MI scaffolds. It is an ECM protein with adhesive activity, upregulated and necessary in a number of developmental contexts, but there are few molecular imprinting studies using this protein. One example is the study performed by D. Zhu *et al.* [56], who used Fn as the template molecule on a polypropylene (PP) non-woven supported calcium alginate/polyacrylamide hydrogel film (PP-s-CA/PAM), via Ultraviolet (UV) radiation-reduced polymerization. The molecularly-imprinted hydrogel exhibited an improvement in terms of adsorption capacity for Fn, compared with the non-imprinted (NI) hydrogel and was successfully used for the culture of

mouse fibroblast cells, exhibiting better cell adherence performance. These results were promising and support the use of Fn for coating or functionalizing materials to promote cellular adhesion [42].

1.5.3. Applications

MI is applied on diverse fields. Chromatography and electrophoresis employ MI to create separation materials. J. -D. Lei and T. -W. Tan [49] studied an affinity chromatography model using MI to explain the retention mechanism, by developing a chiral stationary phase for naproxen separation. The results suggested that racemic naproxen was efficiently resolved on the MIP and the affinity chromatography mechanism controlled the retention in that system.

Chemical sensing can also apply the concept of selectivity and recognition into the development of the materials. A study concerning a sensor based on surface MI was developed by Y. Wang *et al*. [51]. This group applied the method to the detection of carcinoembryonic antigen (CEA), amylase and poliovirus, developing a gold-coated silicon chip. As results of the work, the group could track the production of CEA as a function of cell number and incubation time, the imprinted amylase sensor also demonstrated good selectivity in the real serum test, and the detector was also shown to successfully detect poliovirus.

Drug delivery aims to combine the delivery of a drug in response to some environment triggers, such as the presence of some molecules or biomarkers. F. Puoci *et al*. [67] focused on a controlled release device for 5-fluorouracil, an anticancer drug, especially in gastrointestinal fluids. The authors performed bulk imprinting using methacrylic acid as a functional monomer and Ethylene glycol dimethacrylate (EGDMA) as the crosslinking agent, and evaluated the capacity of the polymer to recognize and to bind the template selectively in both organic and aqueous media. They achieved a more sustained release of the drug, with the MIP binding more 5-fluorouracil than the NIP.

Cell imprinting also calls upon MI knowledge, using the notion that surfaces with defined shape patterns and roughness, replicated from the proliferated cells, can improve cell culturing. Cell imprinting can be used to improve the viability of osteoblast-like cells, which was shown by the work of H. Jeon and G. Kim [68], who used a poly(dimethylsiloxane) surface and osteoblast-like cells as a target cell pattern and constructed cell-imprinted surfaces using an electric field assisted casting method for different culturing times. The cell imprinting was performed by having the fixation of the cells with glutaraldehyde, then culturing the cells on the poly(dimethylsiloxane) surface and finally applying an electric field to obtain accurate cell patterns. Then, on the fabricated surfaces, cells were re-cultured to observe the effect of the surface roughness on the cellular activity. The proliferated cells exhibited unique proliferation patterns with distinctive roughness values and the replicated cell patterns significantly enhanced cell viability, alkaline phosphatase (ALP) activity, and calcium deposition.

Chapter 2 - Molecular Imprinting within hydrogels

This chapter is focused on the MI using hydrogels and the summary of the characteristics and strategies adopted to provide the hydrogels the necessary features to a successful imprinting approach.

Hydrogels are characterized by high content of water in its composition and a swelling behaviour associated (**Figure 2.1**). This swelling can be caused by the solvent uptake or changes in pH and temperature, which is the result of crosslinks, permanent entanglements or ionic interactions [69].
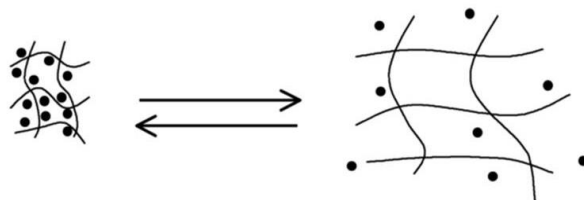
Figure 2.1. Swelling behaviour of hydrogels. During solvent uptake or change in pH or temperature, the polymer mesh suffers an enlargement. **Adapted from** [69]

2.1. Design of hydrogels

Hydrogels are widely studied in TE applications [12], [26], [43], [70]–[73] since their polymeric network can absorb a large amount of water or biological fluid, and has a similar structure to natural ECM. Hydrogels also possess a degree of flexibility similar to natural tissues. The crosslinking structure can be caused by covalent bonding, entanglements, hydrogen bonding or ionic bonding [65]**.**

Hydrogels can be designed for delivery systems [72], [74]–[76], cell encapsulation [45], [77] or for sensor/diagnostic devices [78].
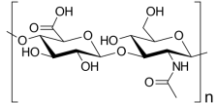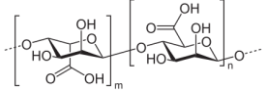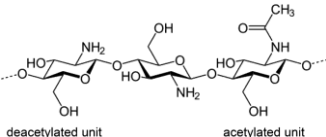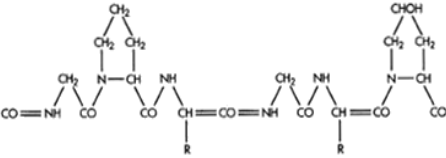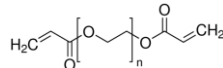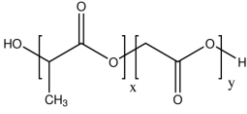
In TE, V. L. Tsang *et al.* [45] took advantage of the proximity of hydrogels with tissues, to develop an hepatic tissue construct using a multilayer photopatterning platform for embedding cells in hydrogels. The group tailored poly(ethylene glycol) (PEG) hydrogels containing the RGD sequence, to support hepatocyte survival and liver-specific function. The results of the group indicated that the photopatterning of hydrogels facilitated the transport of oxygen and nutrients required to the metabolic demands of encapsulated hepatocytes and could be maintained for two weeks in a perfusion bioreactor, setting the aim to further in vitro and in vivo studies.

The next section (2.2) will focus on some examples of polymers chosen for the development of hydrogels.

2.2. Polymers used on the synthesis of hydrogels

Hydrogels can be produced by either natural/biological, synthetic or hybrid polymers, based on their derivation and composition. **Table 2.1** presents examples of these polymers.

Table 2.1. Example of (natural or synthetic) polymers used on the development of hydrogels monomer (Poly(ethylene glycol) diacrylate – PEGDA, Polyvinyl alcohol (PVA))

Name	Chemical Structure	Origin	References
HA		Natural	[26], [27], [79], [80]
Alginate		Natural	[44], [56], [77], [81], [82]
Chitosan		Natural	[24], [32], [83]
Gelatin		Natural	[83], [84]
PEGDA		Synthetic	[45], [72], [85]
PVA		Synthetic	[43]
PLGA		Synthetic	[28]

2.3. Mechanical characterization of hydrogels

The amount of water present in the hydrogel network contribute to the poor mechanical properties of these materials, with elastic modulus values around kiloPascal (kPa) [86]. Their mechanical properties are tuneable through the use of crosslinking agents or by changing the physical and chemical composition of the polymer, such as the concentration of monomers [81].

With the performance of rheological studies, the mechanical properties of the hydrogel can be characterized and reveal the degree of crosslinking, molecular weight, gelation time or the glass transition region [87]. These studies comprise rheological measurements, involving tension, compression, local indentation or frequency based tests such as shear rheometry or dynamic mechanical analysis [74], [86], [87].

Three important parameters used to characterize the network structure of hydrogels (**Figure 2.2**) are the polymer volume fraction in the swollen state (v_2), the molecular weight of the polymer chain between two neighbouring crosslinking points ($\bar{M}_c$), and the corresponding mesh size or pore size (ξ). The polymer volume fraction in the swollen state is a measure of the amount of solvent retained by the hydrogel. $\bar{M}_c$ is the average number of molecular weight between the crosslinking junctions and it is correlated to the degree of crosslinking and polymer diffusion properties. ξ is the distance between two crosslinking junctions. These parameters can be determined theoretically or using experimental techniques.
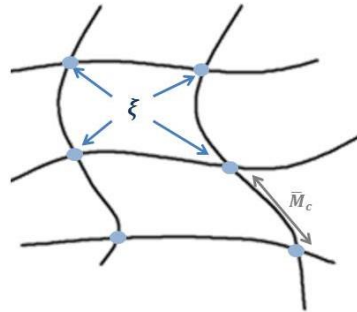
Figure 2.2. Network structure of a hydrogel with the representation of the parameters mesh size (ξ) and molecular weight between crosslinks ($\bar{M}_c$)

The porosity of the scaffold can also be known by the previous measure of the mass and the volume of the scaffold. In **Equation 3** [28], V is the volume of the prepared scaffold and V_p is the volume of the polymer, which is the result of the ratio between the mass and the density of the polymer provided by the suppliers.

$$Porosity = \frac{V-V_p}{V} \times 100 \ (\%) \tag{3}$$

2.4. Imprinting in hydrogels

MI within hydrogels may be more challenging than in rigid structures, due to the expansion of the mesh that can affect the imprinting efficiency by the possible distortion of binding sites. Therefore, MI within hydrogels requires different methodologies.

M. E. Byrne *et al.* [69] outlined a few alternatives for successfully imprinting within hydrogels, based on a biomimetic approach. The group concluded that the macromolecular architecture should be designed differently than other traditional dense networks and have to

include a spatially varying crosslinking density (micro and macroporous regions). One of the alternatives is to include a post-crosslinking reaction, either between excess functional monomers on opposite macromolecular chains or via other monomers introduced into the network, after the gel is formed and the imprint is rebound.

When it comes to design the network architecture for the MI hydrogel, the ratio between crosslinking agents and the functional monomer has also to be considered. Regarding the monomer type and composition, as the molecular mass of the crosslinking increases, the length of the functional monomer should increase accordingly to prevent loss of possible binding regimes due to the swelling or shrinking phenomena [69]. The charge of the monomer or the other components at the time of polymerization may also influence the efficiency of the imprinting, leading to non-specific interactions for all species carrying the opposite charge.

M. Ali and M. E. Byrne [80] developed hydrogel films and contact lenses composed of nelfilcon A, Acrylamide (AAm), *N*-vinyl pyrrolidone and 2-(diethylamino) ethyl methacrylate (DEAEM), imprinted with HA for the controlled release over 24h. Along the study, the group concluded that increasing the total mass content of monomers in the hydrogel influenced the amount and the diffusion rate of HA and the increase of the proportion of DEAEM immobilized more HA within the hydrogel. The trend was that increasing the amount of functional monomer, reduced the cumulative mass of HA released. Also, increasing the diversity of monomers lowered the diffusion coefficient. However, along the study, the mesh size of the hydrogels presented itself uniform.

Concerning the crosslinker, if the amount is too high during the polymerization, it will result in "freezing" of the polymeric chains, restricting their mobility. On the opposite, if it is too low there will be a loss of recognition ability. Crosslinkers, as monomers, should be water-soluble due to the fact that most proteins are water-soluble and uncharged over a relatively wide pH range, in most cases.

2.4.1. Alginate hydrogels

Alginates are naturally occurring anionic and hydrophilic polysaccharides isolated from brown algae such as *Laminaria hyperborea* and *lessonia* [88]. Alginate contains blocks of (1–4)-linked β-D-mannuronic acid (M) and α-L-guluronic acid (G) monomers (**Figure 2.3**). Typically, the blocks are composed in three different forms of polymer segments: consecutive G residues, consecutive M residues and alternating MG residues [89].

These hydrogels can be classified into physical or covalent gels, according to their gelation mechanisms, and they can be prepared under mild conditions. Many methods have been employed for preparing alginate hydrogels, including ionic crosslinking [59], [90], [91], cell-crosslinking or biofunctionalization [92], free radical polymerization [76], [93] and thermal polymerization [77].

The most common method to prepare alginate hydrogels from an aqueous solution is to combine alginate with divalent cations. In the presence of divalent cations, gelation occurs when these cations cooperatively interact with the carboxylic groups of G monomers to form ionic bridges (**Figure 2.3**). Ionic crosslinked alginate hydrogels have been developed and employed in a variety of studies, such as with Ca^{2+} [90], [94], Mg^{2+} [94], or Fe^{2+} [94], [95]. Ca^{2+} is one of the most common divalent cation used to ionically crosslink alginate, providing from calcium chloride ($CaCl_2$) or calcium carbonate ($CaCO_3$) [91]. Alginate and divalent cations can crosslink and form an "egg-box" structure through ionic bond between the cations and ionic G–G sequences along the polysaccharide backbone. However, the speed of gelation is too fast to be

controlled due to the high solubility of calcium chloride in aqueous solution, which limits the application on injectable scaffolds [89].

Other methods of crosslinking alginate are used to promote the stability of the hydrogel, by combining ionically and covalently crosslinking, recurring to photocrosslinking or thermal crosslinking [56], [96]. The advantage of chain polymerization is the variety of chemistries that can be incorporated into the hydrogel by mixing macromers and subsequently copolymerizing.
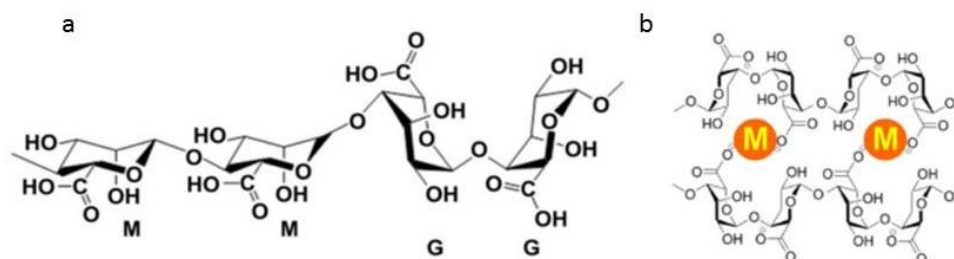
Figure 2.3. (a) Chemical structure of alginate and (b) Ionic interaction between alginate and divalent cations (M) and formation of the "egg-box". **From** [89]

The anionic nature of alginate results in the ability to interact with polyelectrolytes and proteoglycans [89], and the carboxylic groups existence mostly results in a pH responsive behaviour, in which polymers with increasing pH values lead to higher swelling ratios, due to the expansion of the mesh. Also, alginate has on its composition inert monomers that lack informational structure for positive cell biological response, necessary for cell attachment. One strategy is the modification of alginate hydrogels by introducing ligands or peptides [44], [97]. Coupling these peptides helps to control adhesion and results in high specificity to the hydrogel.

Some works developed in MI, using alginate, are presented on **Table 2.2**.

Table 2.2. Overview of some works developed in MI using alginate as a monomer (N,N'-methylenebis(acrylamide) - MBAAm)

Template	Second monomer	Crosslinker	Observations	Reference
BSA	AAm	MBAAm and CaCl$_2$	Film	[55]
BSA	-	CaCl$_2$	Film	[59]
BSA	Sodium poly(acrylate)	CaCl$_2$	Hybrid microspheres	[98]
Cr(III) ions	PVA	Glutaraldehyde	Composite membranes	[99]
Fn	AAm	MBAAm and CaCl$_2$	Film	[56]

Chapter 3 - Aim of the project

Altogether, the previous studies demonstrated that a photocrosslinkable polymer based on the modification of alginate could be done by replacing its functional groups by photosensitive methacrylate groups. Moreover, an improvement on mechanical properties of the alginate hydrogel could lead to better results on the rebinding of the protein, by means of its interface with MI.

Thus, the general objective of this master thesis is to study the effect of different crosslinkers on mechanical properties of the hydrogel and subsequently on the rebinding capacity, to achieve a unique formulation that can confer better recognition to alginate hydrogels. Particularly, the project was developed with the aims of finding how the mechanical properties of the hydrogels could be improved, studying the effect of divalent cations on post-crosslinking of alginate and, finally, performing the studies concerning the protein removal and rebinding to assess the success of the work.

In detail, the previous system developed to produce hydrogels for MI was performed based on photocrosslinkable alginate discs for the recognition of the model protein BSA. First, an alginate modification protocol was optimized to enable the production of methacrylated alginate. The methacrylation was optimized according to the duration, the addition timepoints of the methacrylic compound and the gel formation, using photopolymerization. By the end of the modification, the final solution of methacrylated alginate had the pH adjusted to 5 or 7. Concerning the template removal and the swelling behaviour, the adjustment of the final solution pH to 7 has led to better results.

Chapter 4 - Materials and methods

This section describes the several stages involved in the production of imprinted alginate-based materials, from the modification of the alginate to the protein rebinding tests, starting by the methacrylation of alginate.

4.1. Alginate methacrylation

The first stage of the project was the modification of alginate by methacrylic anhydride (MA) (**Figure 4.1**). Methacrylation of alginate was performed by replacing hydroxyl groups by methacrylate groups (**Figure 4.2**). The addition of functional methacrylate side groups onto the alginate backbone allowed a covalent bonding between chains.
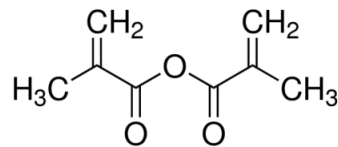
Figure 4.1. Methacrylic Anhydride (sigmaaldrich.com)
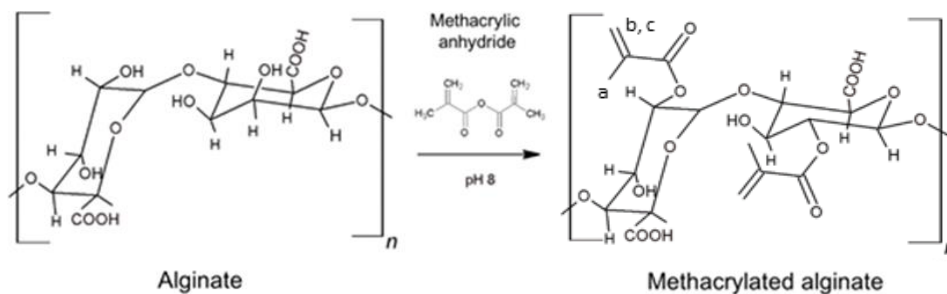
Figure 4.2. Mechanism proposed for the reaction between alginate and methacrylic anhydride. The methacrylation was performed for 10h at pH=8, with the substitution of the available hydroxyl groups on alginate backbone, by methacrylic groups.

Sodium alginate with 70% guluronic acid content (AL, PRONOVA UP MVG, 248.13 kDa, Novamatrix) was dissolved in a Tris(hydroxymethyl)aminomethane Buffered Saline (TBS, pH 8) solution to produce a 1% w/v alginate solution. The alginate methacrylation reaction was performed for 10h by adding MA (154.16 g/mol, Sigma-Aldrich) to the alginate solution in a total proportion of 0.07 g alginate/mL methacrylic anhydride. MA additions were performed at three

different timepoints (0, 3 and 6h). The solution was kept in ice and 5M NaOH (VWR) was added dropwise during methacrylation to keep pH=8 and prevent MA hydrolysis. The assembly of the experiment is represented in **Figure 4.3**.

Figure 4.3. (Left) Assembly of the experiment and (right) pellet recovered after methacrylation.

To stop the reaction, 99% EtOH (4°C) was added in excess to promote polymer precipitation and the pellet (**Figure 4.3**) was left to dry overnight. Rehydration of the pellet was performed by adding deionized water (DI water) under agitation. Dialysis was performed against DI water for 3 days using dialysis membranes (Spectra/Por 3 Dialysis Membrane, MWCO 3.5 kDa). After dialysis, the pH of methacrylated alginate (ALMA) solution was adjusted to 7 using a NaOH solution. The final solutions were frozen at −20°C and lyophilized (Virtris BentchTop Pro 9L −85°C, SPScientific). All the procedure was performed using aluminium foil, to protect samples from light.

4.2. ^{1}H NMR analysis

To perform an analysis on the chemistry of the modification of alginate, unmodified and ALMA were dissolved in deuterium oxide (D_2O, Sigma-Aldrich) to produce a 1% w/v solution. A volume of 5 µl of 3(trimethylsilyl) propionic-2,2,3,3-d4 acid sodium salt (Euriso-top) were added to the solution as internal standard. The Proton Nuclear Magnetic Resonance (^{1}H NMR) spectra was recorded on a BRUKER AVANCE III (400MHz, 9.4 Tesla) NMR spectrometer (Centro de Materiais da Universidade do Porto, University of Porto, Portugal).

The degree of methacrylation (DM) was calculated from ^{1}H NMR spectra based on the ratio of the integrals from the protons of alginate backbone to the protons of methacrylate compound. The final DM was determined by **Equation 4** [77], where a, b and c represent the protons of the methacrylic group on **Figure 4.2**.

$$DM\ (\%) = \frac{Average\left(\frac{H_a}{3} + \frac{H_b + H_c}{2}\right)}{\frac{HAA}{6}} \tag{4}$$

20

4.3. Production of methacrylated alginate non-imprinted and molecularly-imprinted discs

The production of molecularly imprinted materials requires the formation of a polymeric network, where ALMA was the supporting network. In general, such polymeric networks are generated by radical polymerization that unites different small building blocks into larger pieces. Different chemical initiators may be used for this purpose. The present polymerization was started by irradiating a suitable photoinitiator with UV light, which further activated the methacrylate groups within the ALMA structure, to start the polymerization and the formation of covalent crosslinked bonds. Two sources of UV light were used:

1) 320−395nm BlueWave 200 Light-Curing Spot Lamp;
2) 365nm Hamamatsu UV-LED module C11924-221.

Along the project, the effect of two crosslinking agents, EGDMA (198.22 g/mol, Sigma-Aldrich) and MBAAm (154.17 g/mol, Fluka), and a monomer AAm (71.08 g/mol, Sigma-Aldrich), upon the mechanical properties and rebinding efficiency of the alginate discs was assessed (**Figure 4.4**).

To produce prepolymer solutions with 2% or 4% w/v ALMA, the dissolution of ALMA was prepared either in a 0.05% or 0.1% w/v photoinitiator solution, primarily prepared by dissolving 2-hydroxy-1-[4-(hydroxyethoxy)phenyl]-2-methyl-1-propanone (Irgacure 2959, 224.25 g/mol, Sigma-Aldrich) in a 0.9% w/v NaCl solution at pH 4.2. The solution of 0.9% w/v NaCl at pH 4.2 was prepared by adjusting the pH of 0.9% w/v NaCl solution with HCl. Irgacure 2959 (**Figure 4.5**) is a moderately water-soluble radical photoinitiator for the UV curing of systems comprising of unsaturated monomers and prepolymers [100] and was selected for this protocol since it has been reported to cause minimal cellular toxicity in a range of mammalian cell types, amongst others photoinitiators [93], therefore being a safe choice for biomedical applications.

The solutions incorporating crosslinkers were produced by following the above protocol with an extra addition step of either EGDMA, MBAAm, AAm or both MBAAm/AAm in 0.9% w/v NaCl (pH 4.2) with photoinitiator, prior to ALMA addition. The formulations used throughout the work are represented in **Table 4.1**.
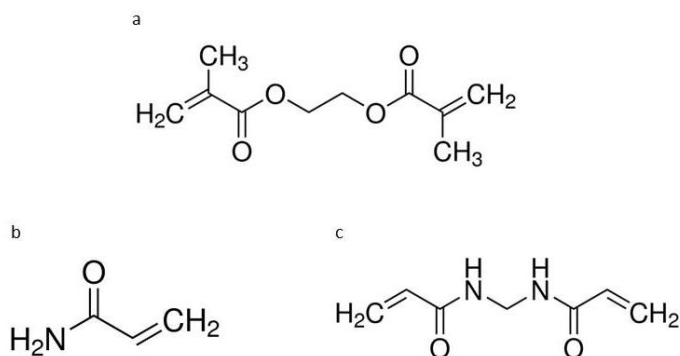
Figure 4.4. Different crosslinking agents and monomer used - (a) EGDMA, (b) AAm and (c) MBAAm (sigmaaldrich.com)

HO—CH₂CH₂—O—(benzene ring)—C(=O)—C(CH₃)(OH)(CH₃)
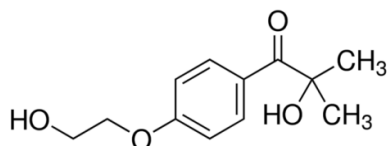
Figure 4.5. Irgacure 2959 (sigmaaldrich.com)

Table 4.1. Different formulations studied throughout the project. The concentrations and formulations highlighted are the ones used for the molecular imprinting protocol.

% ALMA (w/v)	Crosslinker / Monomer			Formulation
	EGDMA	AAm	MBAAm	
2	0mM			
	10mM			
	47mM			
4		0mM	0mM	A
			3mM	B
			9mM	
			12mM	
		3mM	3mM	C
		12mM	3mM	D

The formulations used for preparing MI materials are the ones highlighted in **Table 4.1** (A, B, C and D). For that, the model protein BSA (~66kDa, VWR), was dissolved in the photoinitiator solution (only tested for 0.1% w/v Irgacure) to make a 0.5% w/v BSA solution. After the addition of crosslinker and monomer (3mM MBAAm and 3mM or 12mM AAm), alginate was added to make a 4% w/v polymer solution. Solutions were left mixing at room temperature (RT) for about 30mins.

To produce alginate discs, the same protocol was performed but no BSA was added to the initial Irgacure solution.

Then, 20µL of MIP or NIP solutions were dispensed with a gel pipette to a TEFLON platform, covered with glass while using two 250µm spacers, and exposed to UV light adjusted to a light intensity of 7 mW/cm^2 or 18 mW/cm^2 for 180s or 10min, respectively. This methodology with spacers was used to control the disc dimensions such as thickness and diameter, since the thickness of the spacer used or the volume of solution can be varied.

4.4. Swelling behaviour of alginate discs

Since the swelling of the alginate hydrogels may affect the release of the protein, the swelling behaviour of the discs was evaluated after synthesis and during template removal and

rebinding assays, by the weight variation of discs incubated in solutions of different composition and throughout certain timepoints.

During template removal protocol and rebinding assay, the discs were incubated in a 24-well plate. At each timepoint, the incubation solution of the discs was removed from the wells, the water on the surface of the disc was removed and the discs were weighed.

The weight of alginate discs at different timepoints was measured in an analytical balance (Sartorius CPA225D). The swelling ratio (SR) was calculated according to the **Equation 5**. In this,

$$SR = \frac{m_t}{m_0} \hspace{4cm} (5)$$

m_t (mg) corresponded to the wet weight of the alginate disc at a specific timepoint t, and m_0 (mg) to the weight of the alginate disc immediately after production.

4.5. Morphological analysis by Cryo-SEM

Morphological analysis was performed on discs A and D (**Table 4.1**), using Cryo-Scanning Electron Microscopy (Cryo-SEM). The Scanning Electron Microscopy/Energy Dispersive Spectroscopy (SEM/EDS) exam was performed using a High-Resolution SEM with X-Ray Microanalysis and Cryo-SEM experimental facilities: JEOL JSM 6301F/Oxford INCA Energy 350/Gatan Alto 2500 (Centro de Materiais da Universidade do Porto, University of Porto, Portugal).

ALMA NIP and MIP discs were hydrated in 500 μL DI water for approximately 20h. For the Cryo-SEM assay, samples were cut in small parallelepiped shapes and placed in the support, rapidly cooled (plunging it into sub-cooled nitrogen–slush nitrogen) and transferred under vacuum to the cold stage of the preparation chamber. Samples were fractured, sublimated ('etched') for 100s at −90°C, and coated with Au/Pd by sputtering for 45s. Samples were then transferred into the SEM chamber and studied at a temperature of −150°C.

4.6. Mechanical characterization

To characterize the mechanical properties of crosslinked and non-crosslinked alginate materials, the discs were incubated in a 24-well plate for approximately 24h at 37°C (Incubator Raypa) in a volume of 500μL of each one of the two solutions: Phosphate buffered saline (PBS, pH 7.4) or cell culture Dulbecco's Modified Eagle's Medium (DMEM, Gibco) with 4-(2-Hydroxyethyl)piperazine-1-ethanesulfonic acid (HEPES, 238.30 g/mol, Sigma-Aldrich), pH 7.5. DMEM-HEPES was used to analyse the possible influence of the divalent cations from the DMEM composition, on post-crosslinking of alginate discs.

The shear modulus - elastic component (G', Pa) is a measure of elasticity of the disc and was calculated by the average of the G' values within the linear viscoelastic region (LVR). The

sample was loaded into the instrument and different types of sweep measurements are performed. The strain sweeps are used to determine the maximum strain that delivers a material response within the LVR. In this region, the applied oscillations were non-destructive. On the frequency sweeps, a value within the LVR from the strain sweep was employed, while the oscillation frequency was varied and the strain was held constant.

The rheology studies were performed (n=3) using a Kinexus Pro Rheometer (Malvern Instruments, Malvern) at 37°C in a water-vapor saturated environment ensured by the rheometer chamber using parallel plate geometry (Ø 4mm) and compressing discs by approximately 10% of their height. Samples were prepared and tested by frequency sweep measurements (start frequency 0.01 Hz, ending frequency 10 Hz, constant shear strain rate 1%, points per decade 10) and strain amplitude sweep measurements (start shear strain rate 0.1% or 0.5%, ending shear strain 10%, constant frequency 0.1 Hz, points per decade 10).

The parameters used to characterize the network structure of hydrogels were the polymer volume fraction in the swollen state (v_2), the molecular weight of the polymer chain between two crosslinking points ($\bar{M}_c$), and the corresponding mesh size (ξ), according to S. C. Neves *et al.* [12].

The mesh size of alginate hydrogels, after being swollen in cell culture medium at 37°C, was obtained using the rheometry results to obtain the $\bar{M}_c$, estimated from G' of the swollen alginate discs [101]. First, the discs were incubated in DMEM for 24h at 37°C to reach the swelling equilibrium and, after the incubation the discs were weighed, freeze-dried and weighed again. The swelling ratio (q_F) and polymer volume fraction (v_2) were calculated using **Equations 6** and **7**,

$$q_F = \frac{(mass\ of\ the\ hydrogel\ after\ swelling)}{(mass\ of\ the\ hydrogel\ after\ freeze-drying)} \tag{6}$$

$$v_2 = [1 + (q_F - 1)\,\rho_{AL}/\rho_D]^{-1} \tag{7}$$

where ρ_{AL} is the density of ALMA (0.8755 g/cm^3 [82]) and ρ_D the density of cell culture medium at 37°C (0.99 g/cm^3 [12]). $\bar{M}_c$ was calculated using **Equation 8** [26], [101],

$$\bar{M}_c = c_P RT/G' \tag{8}$$

where c_P is the concentration of alginate in solution (40000 g/m^3), R is the gas constant (8.314 m^3.Pa.mol^{-1}.K^{-1}) and T is the temperature at which the measurement was performed (37°C = 310.15 K). The mesh size (ξ) was then calculated as **Equation 9** [101],

$$\xi = v_2^{-1/3}\, l\, (2\,\bar{M}_c/M_r)^{1/2} C_n^{\,1/2} \tag{9}$$

where M_r is the molecular weight of guluronic acid unit (198 g/mol), l is the length of the repeating unit (4.35Å [102]), and C_n is the Flory characteristic ratio for the polymer ($C_n = 0.021 M_W + 17.95$, where M_W is the alginate molecular weight [70]).

4.7. Template removal

A template removal protocol was developed to maintain the discs integrity along the process, for about 24h.

Briefly, right after production, the discs were incubated in 500µL of 0.05M Tris-HCl (pH 7.4) for 2 cycles of 1h30min each, and posteriorly in DI Water (pH 5.5) for 2 cycles of firstly 3h and secondly 15h. This protocol was developed at RT and under agitation (110 rpm). Template removal was determined by protein quantification (section 4.9).

4.8. Rebinding assay

Rebinding assays were performed to analyse the imprinting features of MIP discs when comparing to the NIP discs. NIP and MIP discs (n=3) were produced accordingly to section 3.3.

Both NIP and MIP discs underwent the same template removal protocol described in section 4.7. After template removal, discs were incubated in 0.1% w/v BSA solution in 0.9% NaCl solution (pH 4.2), similarly to the initial imprinting solution, with agitation (110 rpm) at RT for 28h. Afterwards, samples were tested for protein quantification (section 4.9).

4.9. Protein quantification

The analysis of the protein content, after template removal and rebinding, was performed on the digested discs.

The discs were digested in 200µL of 0.5M NaOH and tested using DC Protein Assay (detection range 0.2−1.5 mg/mL, Bio-Rad) by reading absorbance at 750nm using a Synergy Mx HM550 microplate instrument (Biotek Instruments). The amount of protein present in the disc was calculated by correlating the absorbance values with a calibration curve obtained from standard samples (3 readings *per* sample, and a calibration curve performed for each plate reading). The protein present in the disc (m_{BSA}, µg) was obtained by **Equation 10**,

$$m_{BSA} = \frac{[Abs_{sample} - b]}{a} \times V' * 1000 \qquad (10)$$

where Abs_{sample} (a.u.) corresponded to the relative absorbance value of a sample (i.e., $Abs_{sample\ measured} - Abs_{blank}$), a and b to the constants obtained for the calibration curve (**S1**), $y = ax + b$, where y is in a.u. and x in mg/mL. V' corresponded to the volume of 0.5M NaOH solution (0.2mL) and 1000 was the conversion factor from mg to µg.
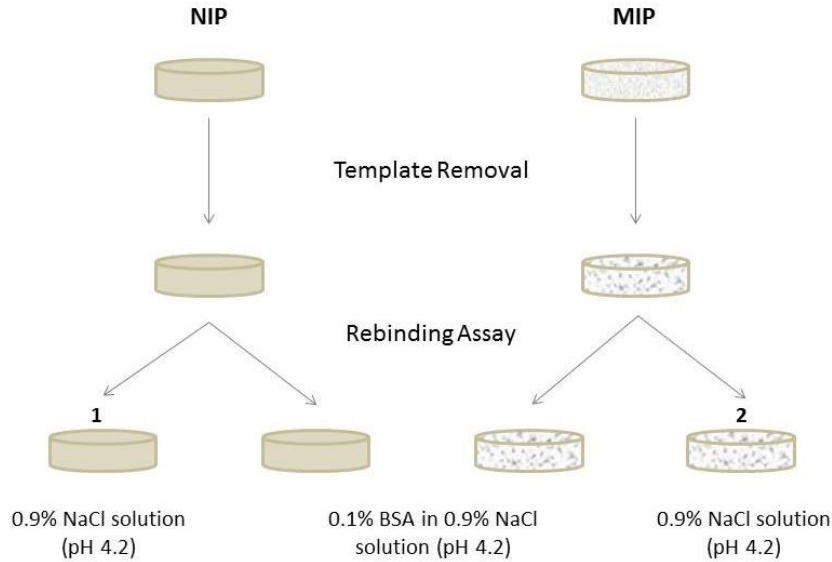
Figure 4.6. Schematic representation of the samples used throughout the molecular imprinting process and the rebinding assay. Disc 1 works as a general control of the molecular imprinting process and an internal control for rebinding assay for NIP discs. On the other hand, disc 2 works as an internal control for MIP discs during rebinding assay. Performing quantifications in relation to disc 1 gives the amount of protein effectively present in discs after the rebinding incubation protocol. In the case of NIP discs, this value corresponds also to Q, while for MIP discs Q can only be determined while performing quantifications in relation to disc 2.

The amount of protein *per* weight of disc, m_{BSA}/m_{disc} (µg/mg) was determined by **Equation 11**,

$$m_{BSA}/m_{disc} = \frac{m_{BSA}}{m_{disc\ wet}} \times SR \tag{11}$$

where SR is the swelling ratio (non-dimensional). Each SR value was used to normalize quantifications as a dilution factor.

The amount of protein removed (%) was obtained by comparing m values obtained for each sample with m_{BSA} measured for MIP discs as produced.

For rebinding analysis (n=3), m_{BSA}/m_{disc} always corresponded to the rebinding capacity (Q) for NIP discs. For MIP discs, m_{BSA}/m_{disc} corresponded to the amount of protein effectively

present in the discs, while Q was obtained following the same equation but determining Abs_{sample} using a different internal control (**Figure 4.6**).

4.10. Statistical analysis

Statistical analysis was performed using GraphPad Prism 6 software for Windows (GraphPad Software, San Diego California USA, www.graphpad.com). The data for each sample was presented as mean value ± Standard Error of Mean (SEM). Statistical differences between groups were performed using t test with Welsh correction. Samples were considered significantly different if P < 0.05.

Chapter 5 - Results and discussion

In this section, the main results of the work are going to be presented and discussed.

5.1. Alginate methacrylation and ^{1}H NMR analysis

It was discussed previously (section 2.4.1.) that the methods used for producing alginate hydrogels can have ionic crosslinking, by combining it with divalent ions, or covalent crosslinking. The drawback in using ionic crosslinking is the lack of physical stability of the gel under physiological conditions, since hydrogels can lose the divalent cations into the surrounding media and suffer degradation [88]. In the context of MI, this lack of stability would also become a problem since the imprinted site of the target protein is expected to have a steady shape.

Photocrosslinking was the crosslinking method used in this project, where covalent bonding between modified alginate polymer chains was induced upon light exposure [81]. For this type of crosslinking, the alginate can be previously modified with groups sensitive to radical polymerization. In this, methacrylate functional groups replace hydroxyl or carboxyl groups of alginate (methacrylation) and are subjected to free radical polymerization after being exposed to UV light in the presence of a photoinitiator [81].

The methacrylation protocol was based on a previous work, in which the reaction with MA was performed for 10h. The mechanism behind the methacrylation reaction is showed in **Figure 4.2**, representing the substitution of the hydroxyl groups in the alginate backbone, by the methacrylate groups of MA.

Both samples of non-modified alginate and modified alginate were analysed by ^{1}H NMR and the efficiency of methacrylation was calculated by **Equation 4**.

Figure 5.1 shows the two NMR spectra, evidencing new resonance peaks appearing in the modified alginate, ALMA, thereby indicating the presence of new proton species resulting from the concerned reaction. The spectrum of the non-modified alginate (**S2**) presents some undefined peaks, around 2.0, 2.3 and 2.7, which do not correspond to the typical spectra [77]. These peaks may represent artefacts or peaks related to protons, resulting from impurities present in the alginate as reagent. This is confirmed by the fact, that ALMA spectrum also presents these peaks, from approximately 1.0 to 1.6 ppm, which are not representative of the modification itself [77].

The new resonance peaks indicative of a successful replacement of hydroxyl groups are the peaks a, b and c. The chemical shift of these peaks is approximately 1.9, 5.7 and 6.1 ppm, respectively (**S3.A**). Using these data and the integration of the peaks, the final degree of methacrylation was calculated as the measure of the result of the degrees of two modifications (**S3**), resulting in approximately 26.8%. This result is in agreement with previous experiments, reported in [77], [81].
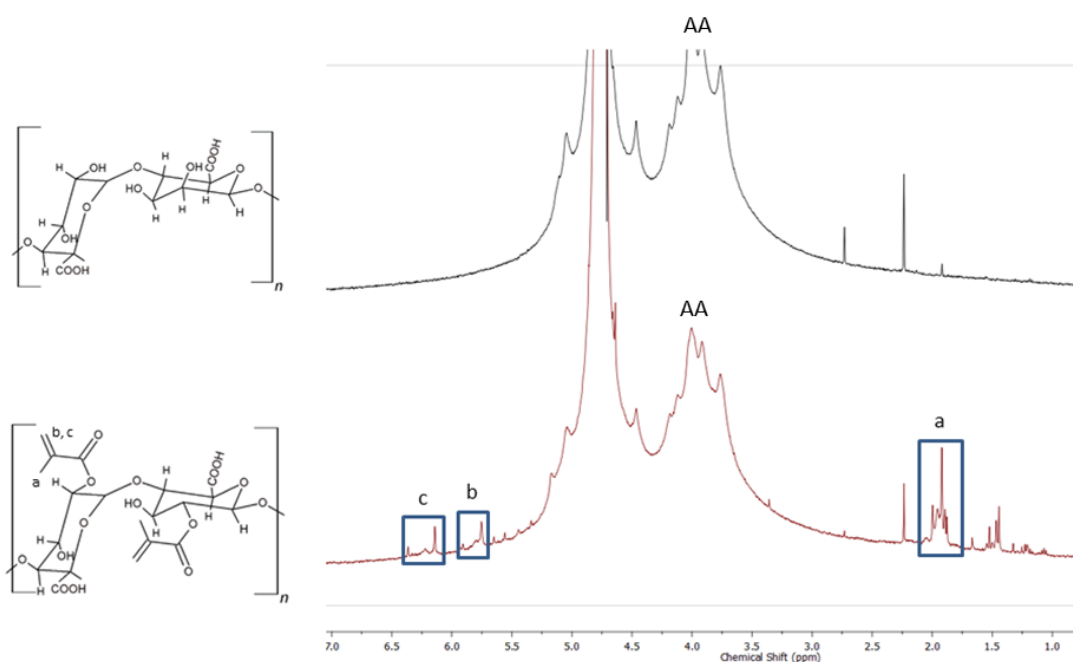
Figure 5.1. Comparison between 1H NMR spectra for non-modified alginate (black) and modified alginate ALMA (red). AA peak represents the protons present on the backbone of non-modified alginate and the peaks a, b and c represent the new protons added into the alginate backbone during methacrylation.

5.2. Discs production and mechanical characterization

Discs were produced according to section 4.3. MIP and NIP pre-polymerization solutions were produced by an aqueous-based approach, using a solution of 0.9% NaCl (pH 4.2) as solvent. This approach was set based on a previous work using the same photocrosslinkable alginate-based system and on the work developed by C. L. Bayer *et al.* [59]. The low pH of the solvent, which is below the isoelectric point (pI) of BSA (pI 4.7-4.9 [103]), allows an ionic interaction between BSA and alginate during the polymerization (at pH 4.2, BSA is positively charged).

Also, each time used for the photo-polymerization was studied and optimized for each UV light source used.

After the production of the discs (**Figure 5.2**), a series of assays concerning the mechanical characterization were performed, aiming to analyse the effect of cell culture medium (DMEM) and the crosslinkers on the stiffness of alginate discs. For all the formulations tested, discs were analysed with rheometry tests. Concerning the formulations with MBAAm and AAm (section 5.2.3.), besides the rheometry tests, discs were also analysed according to the parameters discussed in section 4.6.

For this work, the first aim in using different crosslinkers was to reduce the swelling behaviour associated to the hydrogels that could compromise the rebinding, improving the stiffness of the discs. Secondly, crosslinkers were used to improve the resolution of the cavities,

to enhance the rebinding capacity of the discs. EGDMA was the first attempt to improve the mechanical properties of the discs, followed by the studies concerning MBAAm and AAm.
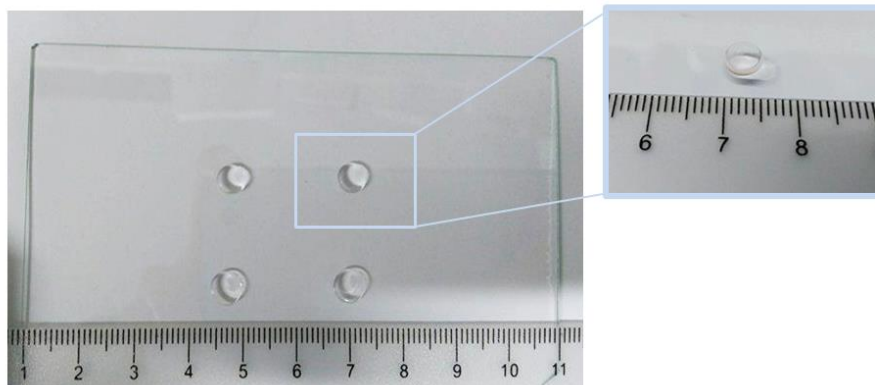
Figure 5.2. ALMA discs right after photo-polymerization, as described in section 4.3.

5.2.1. Post-crosslinking of alginate discs

As discussed in 2.4.1, there are different mechanisms used for the gelation process of alginate solutions, including ionic crosslinking with divalent cations. In this study, the DMEM used in cell culture assays contained magnesium and calcium ions, among other components (vitamins and amino acids) [104], which could interfere with the crosslinking of alginate. In detail, after gel production and incubation, vacant spaces within the hydrogel network could be able to interact with Ca^{2+} or Mg^{2+} from DMEM, turning these two cations into crosslinking agents. This effect was especially relevant because about 70% of the alginate bare structure remained unmodified in ALMA, evidencing that a high number of carboxylic groups would remain available to establish such ionic interaction.

Thus, the effect of cell culture medium DMEM in a possible secondary ionic crosslinking process was tested herein, using ALMA discs only.

This study was important for future work with cells, because the mechanical and morphological characteristics of alginate hydrogels could change during cell incubation, thereby influencing the rebinding capacity and the cellular response to the material. The results obtained are presented in **Figure 5.3** and **S4**.

As expected, the discs incubated in DMEM showed an increase on the storage modulus (G') comparing to the discs incubated in PBS, which corresponded to an increase of the stiffness of the gels. PBS did not contain divalent cations, suggesting that its influence was expressed only on the swelling of the mesh caused by the water uptake.

When the amount of ALMA within the discs was increased from 2 to 4%, the results on G' showed an increase, as well. The fact that more alginate present in the polymer mesh leads to more groups capable of interacting with calcium, the result was a more rigid hydrogel after incubation in DMEM. There was also an increase on G' of the discs incubated in PBS, comparing to discs with 2% in PBS. This was justified by the fact that more alginate present in the polymer mesh leads to an increase of the polymer crosslinking and a more compact

network. This more compact structure hindered the entrance of solvent, thereby diminishing the swelling and increasing the stiffness of the hydrogel.
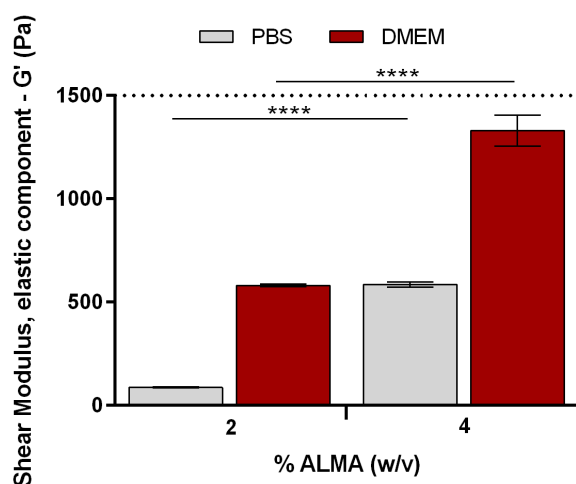
Figure 5.3. Shear modulus – elastic component (G') of alginate discs after 24h incubation in PBS or DMEM. For the tests, the amount of ALMA was varied: 2% and 4% w/v and the amount of photoinitiator (Irgacure 2959) was fixed in 0.05% w/v. Bars represent mean values of n=3 ± SEM and asterisks represent statistical differences (**** $P < 0.0001$). Statistical analysis was performed in comparison with 2% (PBS) and 2% (DMEM) by unpaired t test with Welch's correction.

5.2.2. EGDMA

EGDMA is a difunctional methacrylate (**Figure 4.4.a**) used as crosslinker and monomer for the production of polymeric structures [67], [74]. Its effect on the mechanical properties and swelling of the alginate discs was investigated by varying the concentration of EGDMA (10mM and 47mM) within the 2% w/v ALMA solution and the photoinitiator concentration. The discs (with and without EGDMA) were produced by exposing these to UV light 1 (section 4.3) for 180s. The results of the mechanical properties and the swelling behaviour of the discs after 24h incubation in DMEM are presented in **S5** and **Figure 5.4**, and **Figure 5.5**, respectively.

In general, the results evidenced that, the crosslinked discs produced with the same amount of Irgacure (0.05% in **Figure 5.4.A** and **Table 5.1**) had their mechanical properties decreased in the presence of EGDMA, most evidently in the case of 10mM EGDMA. The interaction within the structure of these gels (between ALMA and EGDMA) could lead to a water uptake into the cavities, turning the gels more suitable for swelling and less suitable for the increase of stiffness. This means that the presence of EGDMA into the structure could decrease the degree of compaction of the mesh.
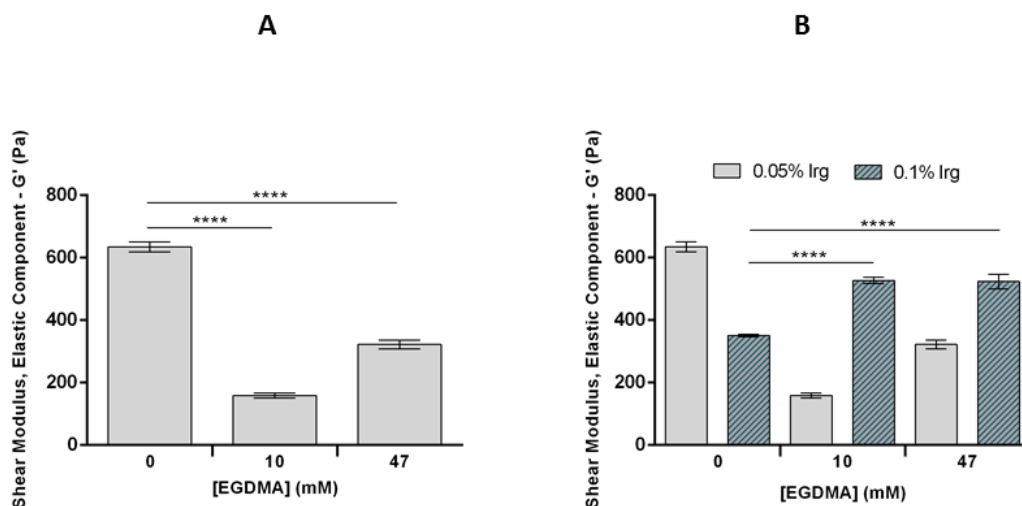
Figure 5.4. Shear modulus (G') of alginate discs crosslinked with 10mM or 47mM EGDMA, and non-crosslinked discs after 24h incubation in DMEM. For the tests, the amount of ALMA was fixed in 2% and the amount of Irgacure was varied: 0.05% (A) and 0.1% (B). Bars represent mean values of n=3 ± SEM and asterisks represent statistical differences (**** $P < 0.0001$). Statistical analysis was performed by unpaired t test with Welch's correction.

Table 5.1. Shear modulus for the crosslinked discs with EGDMA and non-crosslinked discs (0mM) after 24h incubation in DMEM. For the tests, the amount of ALMA was fixed in 2% and the amount of photoinitiator was varied: 0.05% and 0.1%. Data represents mean values of n=3 ± SEM. Data corresponds to data shown in **Figure 5.4**.

EGDMA (mM)	G' (Pa)	
	0.05% Irgacure	0.1% Irgacure
0	634.9 ± 16.3	351.0 ± 3.9
10	159.2 ± 7.9	527.2 ± 10.5
47	322.3 ± 13.7	523.5 ± 23.6

When the amount of photoinitiator was increased (**Figure 5.4.B**), non-crosslinked discs had a decrease on the G', an unexpected result, probably justified by the fact that more Irgacure molecules remained within the ALMA structure, which would enable more defect spaces (spaces occupied by Irgacure), thereby decreasing the stiffness of the discs when incubated in solvent. The unreacted Irgacure molecules, during solvent uptake, could leave the mesh structure of ALMA, leading to a less rigid polymer.

However, there were no significant differences between the swelling of the gels produced with both photoinitiator concentrations, as represented in **Figure 5.5**. In fact, both concentrations of crosslinker showed higher values of swelling, comparing to non-crosslinked discs. Some of these results are related to the stiffness, since the discs with EGDMA with lower

G', presented higher swelling value. However, the same tendency did not happen for the crosslinked discs produced with 0.1% Irgacure, which showed higher swelling and higher stiffness, comparing to the discs with 0mM EGDMA. These results concerning the swelling behaviour of the discs are inconclusive, but evidences of how the mesh is affected by the amount of crosslinker and photoinitiator. In fact, the swelling behaviour along the time of incubation is not represented herein, which could give more information about the swelling equilibrium of the discs. Also, the discs were incubated only in DMEM, so the results showed are mostly the result of a combined crosslinking reaction where the divalent cations in DMEM played an interfering role.
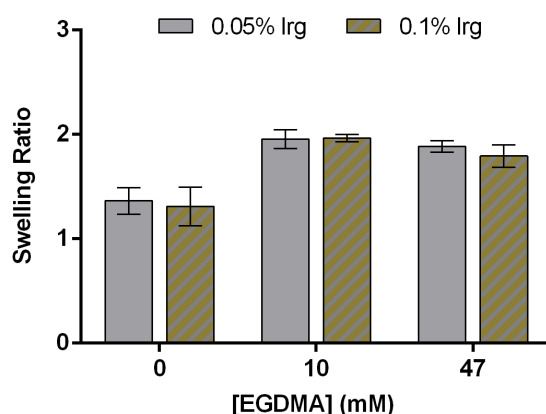
Figure 5.5. Swelling ratio of crosslinked and non-crosslinked alginate discs after 24h incubation in DMEM. The amount of ALMA was fixed in 2% and the amount of photoinitiator was varied: 0.05% and 0.1%. Bars represent mean values of n=3 ± SEM.

Overall, discs produced with EGDMA did not lead to satisfactory results, regarding the good mechanical properties and high rebinding capacity pursued herein. Thus, this crosslinker was evaluated only at this stage and left out in further studies. Its limited solubility could compromise the imprinted features of the final polymer, by hindering the formation of suitable imprinted cavities, which could be destroyed throughout the template removal and rebinding studies.

5.2.3. MBAAm and AAm

To improve the mechanical properties of the alginate-based discs, the effect of other crosslinker and monomer combination was tested: MBAAm and AAm, to understand the interaction of this monomer and crosslinker combination with alginate. In fact, these crosslinkers are widely used in the development of crosslinked polymers with good mechanical properties [50], [56], [61].

First, preliminary studies were performed to understand the amount of ALMA and photoinitiator that led to hydrogels capable of maintaining the integrity throughout template removal and rebinding studies (**S6** and **Figure 5.6.A**), and then studies on the mechanical properties of discs with the addition of crosslinker. These last studies are represented in **Figures 5.6.B** and **5.7** and **Table 5.2**.
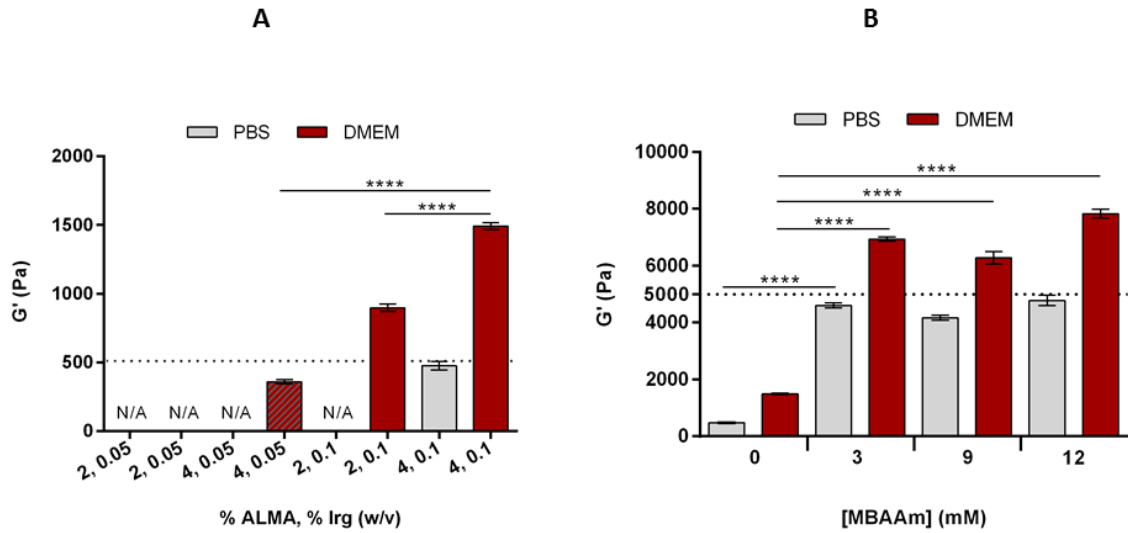
Figure 5.6. Shear modulus (G') of crosslinked and non-crosslinked discs after 24h incubation in PBS or DMEM. In A, the amount of ALMA was varied (2% and 4%) and the amount of Irgacure (0.05% and 0.1%). In B, the amount of MBAAm was varied in a 4% ALMA and 0.1% Irgacure solution. Bars represent mean values of n=3 ± SEM and asterisks represent statistical differences (**** $P < 0.0001$).

Figure 5.7. Shear modulus (G') of crosslinked and non-crosslinked discs after 24h incubation in PBS or DMEM. In A, the amount of AAm was varied and the discs were produced with 4% ALMA and 0.1% Irgacure. In B, the discs were produced with MBAAm and AAm, with 4% ALMA and 0.1% Irgacure, and the data corresponds to the formulations shown in **Table 5.2**. Bars represent mean values of n=3 ± SEM.
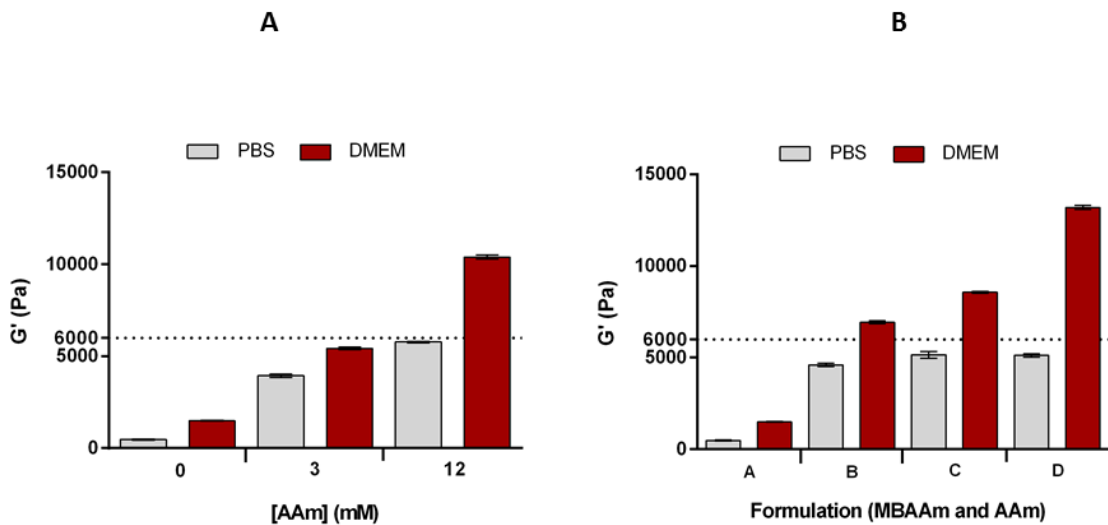
Table 5.2. Shear modulus (G') for the crosslinked discs and non-crosslinked disc after 24h incubation in PBS or DMEM. For the tests, the amount of ALMA was fixed in 4% and the amount of photoinitiator in 0.1%. Data represents mean values of n=3 ± SEM. Data corresponds to results shown in **Figure 5.6.B** and **Figure 5.7**.

AAm	MBAAm	G' (Pa)	
		PBS	DMEM
0	0	475.8 ± 31.6	1493.0 ± 24.6
	3	4602.0 ± 91.6	6936.0 ± 76.5
	9	4168.0 ± 82.2	6283.0 ± 223.4
	12	4781.0 ± 185.5	7832.0 ± 163.8
3	0	3938.0 ± 97.1	5436.0 ± 71.6
	3	5151.0 ± 180.8	8564.0 ± 45.7
12	0	5779.0 ± 44.7	10397.0 ± 106.9
	3	5125.0 ± 94.8	13195.0 ± 115.1

Figure 5.6.A shows the values of G' of the discs with no crosslinker produced by varying the concentration of ALMA (2% and 4%) and Irgacure (0.05% and 0.1%), and exposing the polymer solutions to the UV light source 2 (section 4.3) for 10min. After production, discs were incubated in PBS or DMEM for 24h. After the incubation, discs produced with 2% ALMA and 0.05% Irgacure disintegrated during manipulation and were not able to undergo the mechanical studies. The same happened to discs with 2% ALMA and 0.05% Irgacure incubated in PBS. As for the discs with 4% ALMA, only the discs with 0.05% Irgacure incubated in PBS did not undergo the mechanical studies. Therefore, the discs were produced with 4% ALMA and 0.1% Irgacure.

Figures 5.6.B and **S7**, and **Figure 5.7.A** and **S8** represent the results of the mechanical properties of the discs produced with MBAAm and AAm, respectively. Both compounds significantly improve the stiffness of the discs and DMEM is again a factor responsible for further increase the stiffness of all the discs. Discs produced with MBAAm showed a tendency for maintaining similar values of G' for different concentrations, after PBS and DMEM incubations. This tendency eased the choice of the concentration used for further improvement of the system. For formulations with both compounds, the concentration of MBAAm chosen was 3mM, since it was the lowest concentration studied and since the mechanical properties were very similar, between the three concentrations.

When the amount of AAm was increased from 3 to 12mM, the increase on G' was more significant than on discs crosslinked with MBAAm. MBAAm has higher molecular weight than AAm, which means that the bonding between the functional groups of MBAAm and ALMA will have a bigger length, allowing the formation of pores with a bigger size. With a structure presumably with wider pores during swelling, the expansion of the mesh will be higher for ALMA/MBAAm resulting in a lower stiffness, comparing to ALMA/AAm discs.

For these reasons, discs were further prepared with 3mM or 12mM of AAm and 3mM MBAAm, and the results are shown in **S9** and **Figure 5.7.B**. The discs represent the conditions tested for molecular imprinting protocol (**Table 4.1**) and comprise discs with both AAm and MBAAm, discs with only MBAAm and discs with no crosslinker. The interesting part in these results is that all the crosslinked discs showed the same tendency in G', when incubated in PBS. The major difference occurs when the discs were incubated in DMEM, which resulted in discs D (12mM AAm and 3mM MBAAm) having bigger shear modulus than discs B and C (3mM MBAAm and 3mM AAm/3mM MBAAm, respectively). **Figure 5.8** represents the disc D used for the rheometry tests, after 24h incubation in PBS or DMEM. As seen, there is no significant swelling after the incubation, although the disc incubated in PBS appeared more swollen than the disc incubated in DMEM, as expected since it had lower G'.

Figure 5.8. NIP discs produced with 12mM AAm and 3mM MBAAm, right after production (first disc) and after 24h incubation in PBS or DMEM. Each disc was inside a well in a 24-well plate. Scale bars represent 200mm.

AAm polymerization (formation of polyacrylamide) is commonly used for the preparation of gel for electrophoresis [105] or other hydrogels [56], using MBAAm as crosslinking agent. Different initiators may be employed for this purpose. The most common is a combination of APS and *N,N,N',N'*-Tetramethylethylenediamine (TEMED). Other works, as M. Uygun *et al.* [106], use Ag nanoparticles combined with Irgacure as a source of free radicals. In the present work, only Irgacure was used as radical source after irradiation of UV light.

When discs were prepared with AAm and MBAAm, altogether with the crosslinking of ALMA, the photoinitiator radicals could favour the formation of polyacrylamide in some regions of the chemical structure, forming a hydrogel with different degrees of crosslinking. This heterogeneity could assist the free G blocks of alginate to form a post-ionic crosslinking with calcium and magnesium, during incubation of the discs in DMEM. This heterogeneity was not clear in the discs incubated in PBS, since this solution did not influence the crosslinking of ALMA, but the swelling behaviour of the gels.

Two of these formulations (**Figure 5.7.B**) were morphologically characterized by Cryo-SEM and all the four were characterized by the parameters concerning the mesh of the hydrogel. **Figure 5.9** shows the images obtained with Cryo-SEM and **Table 5.3** presents the results of the parameters calculated according to **Equation 6-9**.

For the morphological analysis, non-crosslinked discs (**Figure 5.9.A-B**) and crosslinked discs D, with AAm and MBAAm, (**Figure 5.9.C-D**) were characterized by electron microscopy.

In this, the two formulations showed significantly different morphologies. Macro-pores and regions with micro-pores were observed in non-crosslinked discs, while the crosslinked discs evidenced pores smaller than 7μm, and a morphology that was closer to a film than to a hydrogel. These thicker pores are probably related to the stiffness of the gels, which was around 10 times higher than the non-crosslinked discs, when incubated in PBS.

All the samples underwent the same preparation for the characterization, but the unexpected morphology obtained for crosslinked discs can be justified by the presence of some salts in the sample or even its formulation with AAm and MBAAm that did not allow the sample to fully freeze and then sublimate. This is a possibility for these results, but no major conclusions could be further considered, because the process of this characterization can be very harsh for the structure of the sample.

The mesh parameters calculated for all the formulations (A, B, C and D) are shown in **Table 5.3**. It was possible to conclude that as the G' increases, the mesh size of the polymer decreases. In fact, the calculations of these parameters required a previous incubation of the discs in DMEM, which further improved the stiffness of the discs. The high degree of crosslinking in the mesh could contribute for less expansion of the mesh. A less expansion could then be translated in the formation of smaller pores. The mesh size for the non-crosslinked discs was in resonance to results found in [70].
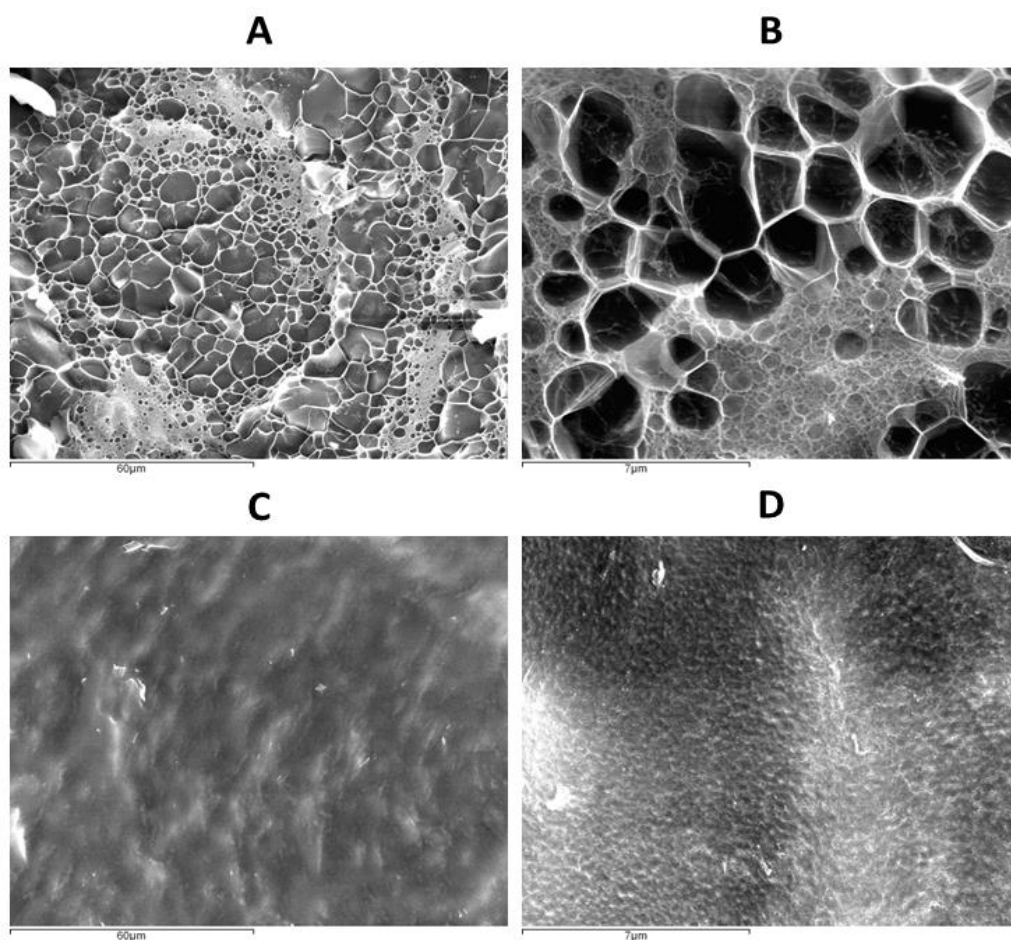

Figure 5.9. Representative Cryo-SEM images of NIP non-crosslinked discs (A and B), and discs with 12mM AAm/3mM MBAAm (C and D). Scale bars represent 60μm (A and C) and 7μm (B and D).

Table 5.3. Shear modulus (G'), volume fraction in the swollen state (v_2), molecular weight of the polymer chain between two crosslinking points ($\bar{M}_c$) and mesh size (ξ) of the NIP formulations A to D, represented in **Figure 5.7.B**, after 24h incubation in DMEM. Data represents mean values of n=3 ± SEM.

Formulation	G' (Pa)	v_2	$\bar{M}_c$ (g/mol)	ξ (nm)
A	1493.0 ± 24.6	0,051 ± 0.008	69107.9	152.7 ± 8.4
B	6936.0 ± 76.5	0,056 ± 0.002	14870.9	67.6 ± 0.7
C	8564.0 ± 45.7	0,069 ± 0.003	12043.3	56.9 ± 0.9
D	13195.0 ± 115.1	0,069 ± 0.004	7817.1	45.7 ± 0.9

5.3. Template removal analysis and protein quantification

The imprinting is established when polymerization is occurring in the presence of a protein, acting as the template. Once the polymerization is concluded, the protein template must be extracted from the polymeric matrix, leading to the formation of rebinding positions. For this purpose, an inverse approach to the preparation of the pre-polymerization solutions was selected; the pH was raised above the pI of BSA to break the ionic interaction between BSA and ALMA (both components are negatively charged). This was done by incubating the discs in 0.05M Tris-HCl (pH 7.4) and then in DI water.

Figure 5.10 and **Table 5.4** present the results related to the template removal, in the same conditions as for the MI protocol (**Table 4.1**). This data was obtained by the digestion of the discs and subsequent analysis of the protein content in the digested sample.

It was possible to observe that the percentage of BSA removed tended to stabilize throughout the experiment, for all the conditions studied. Overall, results suggested that some BSA molecules could exit the polymer matrix easily, while others were irreversibly entrapped into the bulk polymer.

At the first 3h of the incubation, the discs 3:3 showed the highest template removal with an average percentage of 63.8%. Throughout the template removal, the 12:3 were the discs with less amount of BSA removed, with 41.5% at the first 3h.

Template Removal

AAm:MBAAm (mM)

■ 0:0 ▨ 0:3 ■ 3:3 □ 12:3
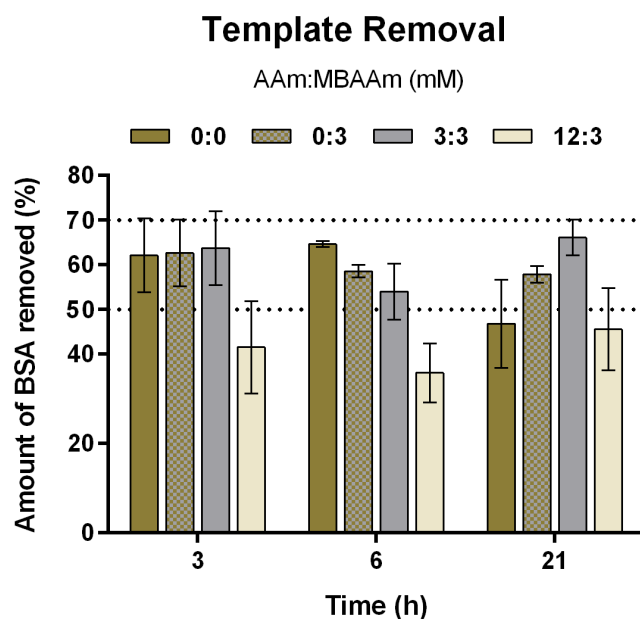
Figure 5.10. Percentage of template removal by protein quantification in MIP discs. Bars represent mean values of n=3 ± SEM.

Table 5.4. Amount of BSA in the discs and percentage of template removal by protein quantification in digested discs. Data corresponds to mean values n=3 ± SEM and to **Figure 5.10**.

AAm:MBAAm (mM)	Time (h)	0	3	6	21
0:0	m_{BSA} in disc (µg/mg)	4.17 ± 0.50	1.58 ± 0.35	1.47 ± 0.03	2.22 ± 0.41
	Removed template (%)	-	**62.1 ± 8.3**	**64.7 ± 0.7**	**46.8 ± 9.8**
0:3	m_{BSA} in disc (µg/mg)	6.57 ± 0.01	2.45 ± 0.49	2.72 ± 0.09	2.77 ± 0.12
	Removed template (%)	-	**62.7 ± 7.5**	**58.6 ± 1.4**	**57.9 ± 1.9**
3:3	m_{BSA} in disc (µg/mg)	4.08 ± 0.33	1.43 ± 0.22	1.84 ± 0.16	1.49 ± 0.15
	Removed template (%)	-	**63.8 ± 8.2**	**54.0 ± 6.2**	**66.1 ± 3.9**
12:3	m_{BSA} in disc (µg/mg)	4.45 ± 0.63	2.48 ± 0.26	2.39 ± 0.30	2.35 ± 0.37
	Removed template (%)	-	**41.5 ± 10.3**	**35.8 ± 6.6**	**45.6 ± 9.2**

The template removal of the non-crosslinked discs (0:0) did not significantly differ from the other conditions. This may be justified by the amount of ALMA (4%) used for the preparation of the discs, which could be very high to allow the exit of the protein. Furthermore, this would also suggest that an increased crosslinking effect, promoted by the presence of AAm and/or MBAAm in the polymerization stage, did not impact upon the template removal, except for the 12:3 AAm:MBAAm ratio.

Considering the results high deviations, these data presented itself difficult to analyse. One reason could be the fact that the amount of protein present in the discs started reaching the detection range of the protein assay kit used to perform these quantifications, as the template removal would go further in time.

Still, this data is partially in agreement with the swelling profile of the discs during template removal (**Figure 5.11**). The first 3h were more important for the template removal, since the next timepoints (6h and 21h) did not add more information (except for the control material, with 0:0 ratio, where the swelling ratio almost doubled from 3 to 21 hours). As in the swelling, this removal behaviour was also visible, since the increase on the swelling ratio for the first 3h was more significant than in the rest of the removal. This rapid swelling could be explained by the entrance of solvent, which lead to the exit of BSA. In fact, considering the results of the discs shear modulus in PBS (**Table 5.2**), which is close to the Tris-HCl solution, the discs with higher G' showed a lower swelling, as the 0:3, 3:3 and 12:3 discs. **Figure 5.12** shows the 3:3 discs during three timepoints of the template removal (0h, 3h and 21h). Between MIP and NIP, there were no significant differences considering the swelling and the integrity of the discs, which remained throughout all the washing process.

These results on the percentage of template removal can also be linked to the obtained results for the mesh parameters. Although these last results report quantitative data, they do show the tendency of the mesh to swell and to even release the protein. Both results lead to the notion that lower pore size yields lower swelling, which can influence the removal of the protein.
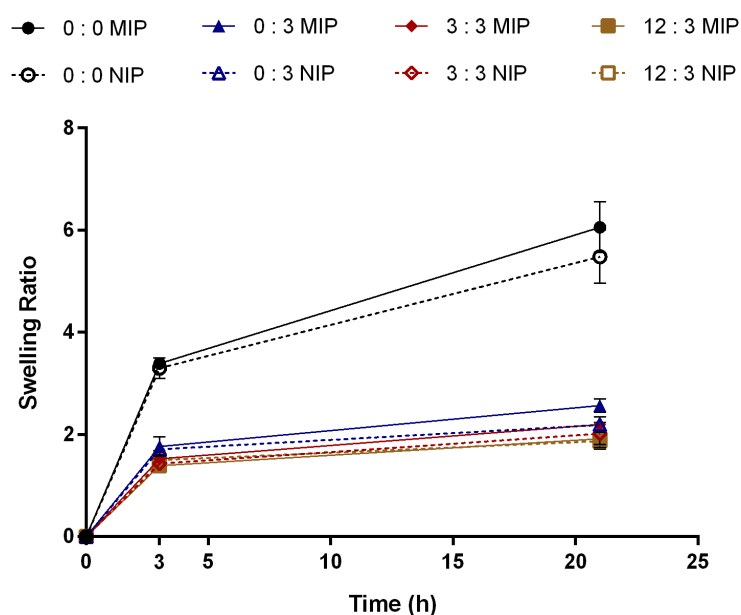

Figure 5.11. Swelling profile of MIP and NIP discs during template removal protocol. Maximum swelling was achieved at the end of the template removal (t=21h). Data represent mean values of n=3 ± SEM.
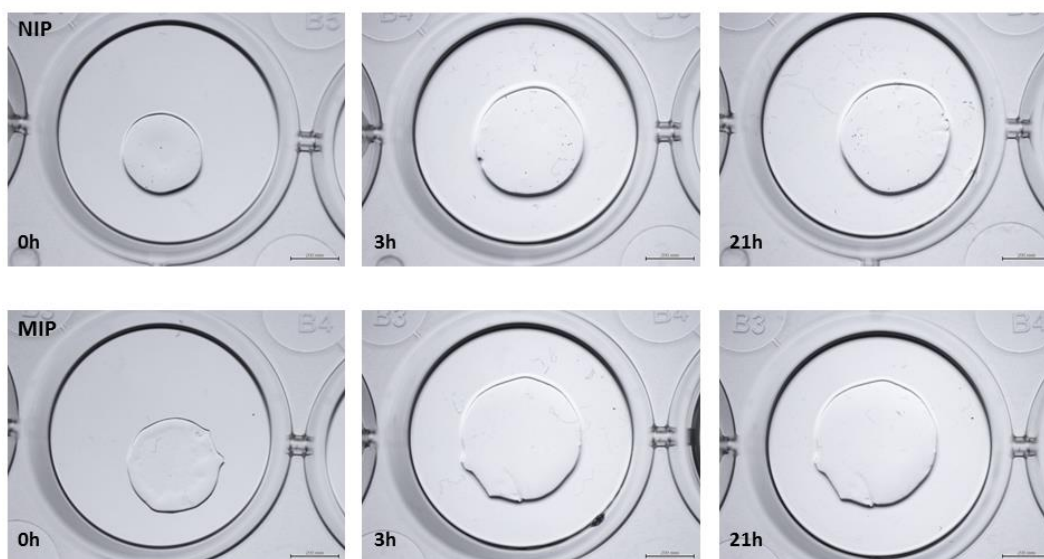
Figure 5.12. NIP and MIP discs produced with 3mM AAm and 3mM MBAAm, during the template removal (timepoints 0h, 3h and 21h). Each disc was inside a well in a 24-well plate. Scale bars represent 200mm.

5.4. Rebinding studies and protein quantification

Rebinding studies were performed to characterize and compare the capacity of MIP and NIP (crosslinked and non-crosslinked) discs to adsorb the template molecule, using two molecular imprinting parameters: rebinding capacity (Q, µg/mg, **Equation 1**) and the imprinting factor (IF, **Equation 2**).

For this, discs were incubated for 28h at RT in two solutions: 0.1% BSA in 0.9% NaCl solution (pH 4.2) or only 0.9% NaCl solution (pH 4.2).

In this part of the work, two different results were analysed, the amount of protein within the discs and the amount of protein effectively adsorbed by the discs. Since none of the discs (conditions tested) achieved fully template removal, which is typical for a MIP material, the amount of the protein within the disc gives the information about the amount of protein adsorbed and the protein that remained after template removal. On the contrary, the amount of protein adsorbed during the rebinding assay was determined by excluding the influence of any protein remaining inside the discs after template removal, corresponding to the rebinding capacity. Based on the values of amount of protein adsorbed by MIP and NIP discs, IF was also determined. For NIP discs, both concepts (amount of protein contained in discs and amount adsorbed by discs) correspond to the same value as these discs were never in contact with any protein until this stage of rebinding.

Throughout the time, the swelling profile was also characterized for each condition, represented in **Figure 5.13**.

After template removal (21h), it was visible that all the discs suffered a deswelling phenomenon, when incubated in the rebinding solution. As it was discussed previously, the anionic nature and the existence of carboxylic (COO^-) groups on alginate structure, lead to a hydrogel with pH-responsive behaviour. This was highly seen in these results: during the

42

template removal, in a basic environment (Tris-HCl, pH 7.4 and DI water, pH 5.5), all the discs suffered swelling and released the protein by the breakage of its ionic bond with ALMA; during rebinding assay, in an acidic environment (0.9% NaCl solution, pH 4.2), all the discs suffer a constriction resulting in even lower swelling ratios than the initial ones. The low pH means a higher presence of H^+ in the solution, which interacted with the COO^- groups. As pH decreased, alginate COO^- groups became protonated (COOH), bearing neutral charge and reducing the electrostatic repulsions, with subsequent contraction of the polymeric chains, decreasing the water uptake and the swelling.
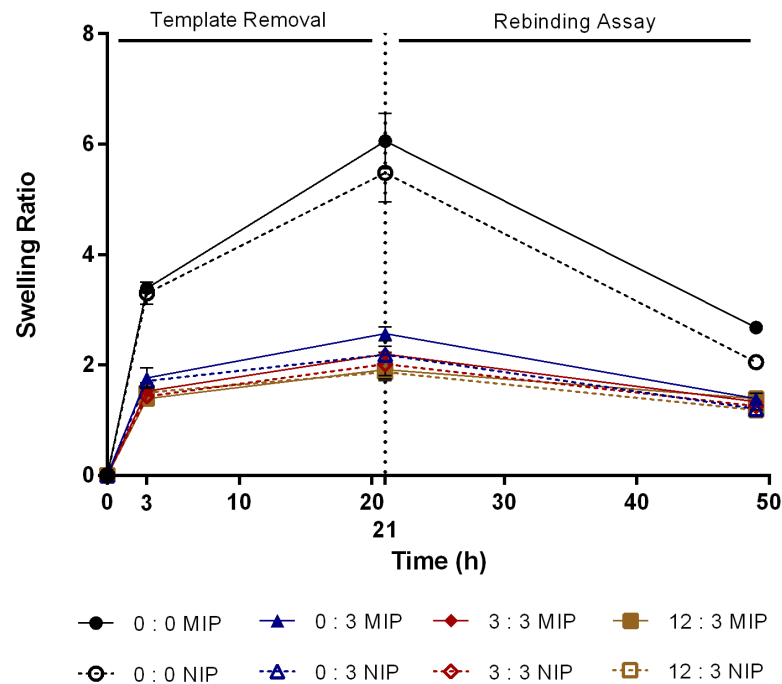
Figure 5.13. Swelling profile of MIP and NIP discs during template removal (21h) and rebinding protocol (28h), total of 49h. Rebinding assay corresponds to incubation of the discs in 0.1% BSA in 0.9% NaCl solution (pH 4.2). Data represents mean values of n=3 ± SEM.

The amount of BSA present in the disc during the rebinding protocol (**Figure 5.14** and **Table 5.5**) showed that MIP discs had a much higher amount of protein inside, due to the protein that was not removed from the disc, and NIP discs had a lower amount of protein, very stable throughout time. The results for the MIP discs (0:0, 0:3, 3:3 and 12:3) were very similar, although in the first hour, 12:3 MIP discs had the smallest amount of protein inside the disc. This means that since it was the disc with lower template removal, the amount of adsorbed BSA was also the lowest, only 1.341 µg/mg. However, this disc had the amount of protein adsorbed constantly increased. Since it was the most crosslinked disc and the disc with lower pore size, probably, the protein was not being adsorbed to the disc in the very beginning of the rebinding assay, but throughout the time.
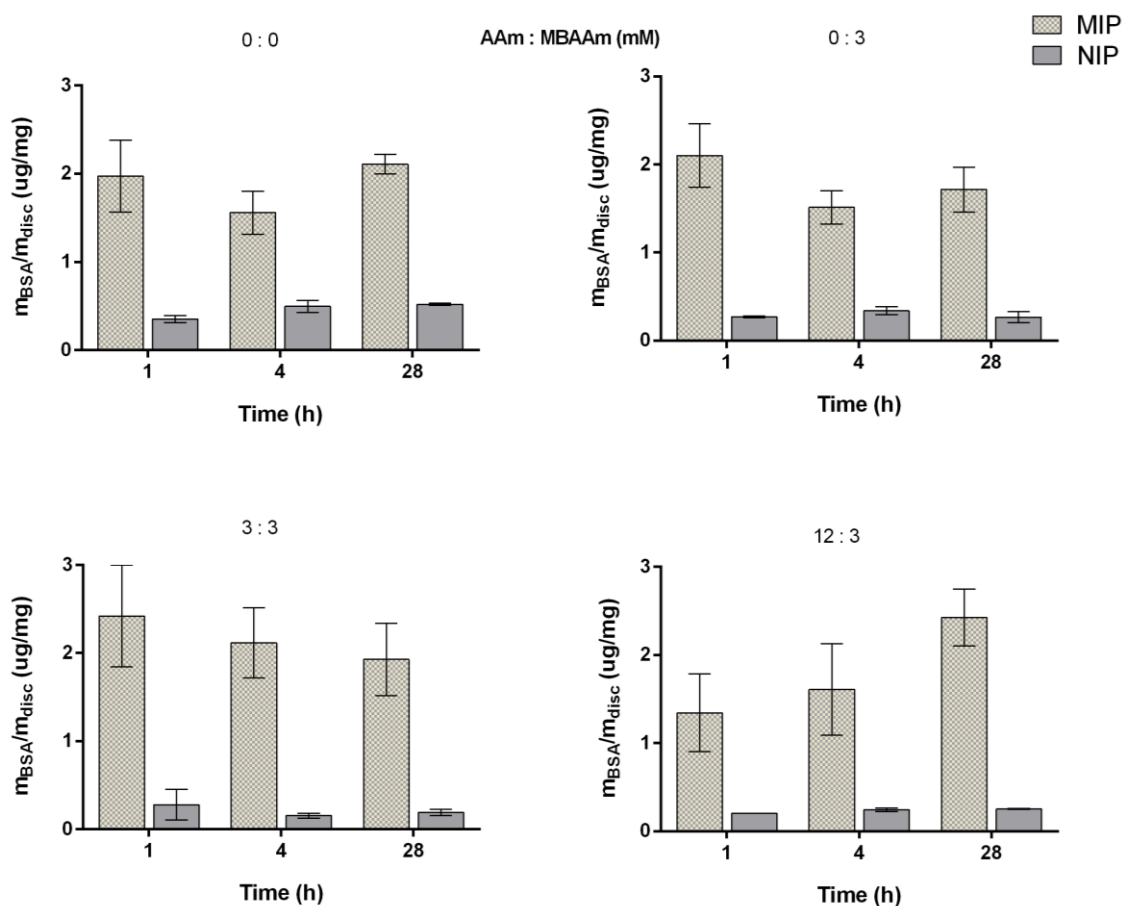
Figure 5.14. Amount of BSA present in MIP and NIP discs during rebinding and incubation in 0.1% BSA solution in 0.9% NaCl (pH 4.2). Bars represent mean values of n=3 ± SEM.

Table 5.5. Amount of BSA present in MIP and NIP discs after 28h incubation in 0.1% BSA solution. Data represents mean values of n=3 ± SEM and corresponds to **Figure 5.14**. (* values of n=1)

AAm : MBAAm (mM)		Amount of BSA in the disc (µg/mg) in each timepoint		
		1h	4h	28h
0 : 0	NIP	0.354 ± 0.040	0.497 ± 0.069	0.519 ± 0.013
	MIP	1.973 ± 0.406	1.559 ± 0.242	2.108 ± 0.113
0 : 3	NIP	0.271 ± 0.008	0.339 ± 0.045	0.267 ± 0.063
	MIP	2.102 ± 0.359	1.514 ± 0.190	1.716 ± 0.256
3 : 3	NIP	0.279 ± 0.173	0.153 ± 0.029	0.191 ± 0.037
	MIP	2.421 ± 0.578	2.117 ± 0.400	1.929 ± 0.409
12 : 3	NIP	0.202 ± *	0.243 ± 0.021	0.252 ± 0.007
	MIP	1.341 ± 0.441	1.608 ± 0.517	2.425 ± 0.321

NIP discs also showed the ability to adsorb protein in the rebinding assays, but only for a small amount. The reason relies on the natural adsorption of the material to the protein; the protein is a multi-charged species and may randomly interact with specific parts of the ALMA structure, modified or not. The higher values of protein adsorption by NIP materials were shown by 0:0 discs (0.354 µg/mg, 0.497 µg/mg and 0.519 µg/mg). This meant that the imprinting approach established by adding monomer and/or crosslinking agents limited the adsorption ability of ALMA.

The rebinding capacity (Q) and the imprinting factor (IF) were also quantified, and the results are shown in **Figure 5.15** and **Table 5.6**. In this study, the control of the system was disc 2 (section 4.9, **Figure 4.6**). As it was observed, all the MIP discs had the highest values of protein adsorbed, although that increase was most notorious for 0:0 and 12:3 MIP discs, which had a protein content of 0.955 µg/mg and 0.494 µg/mg, respectively. In fact, both conditions had the highest IF values, as well. Still, it is important to highlight that 0:0 NIP discs also displayed the highest adsorption values, meaning that the highest non-specific rebinding was occurring in this material and that the presence of monomer/crosslinker contributed to diminish such effect. In general, the material with best recognition features was the 12:3 MIP disc, with an imprinting factor of 1.98.
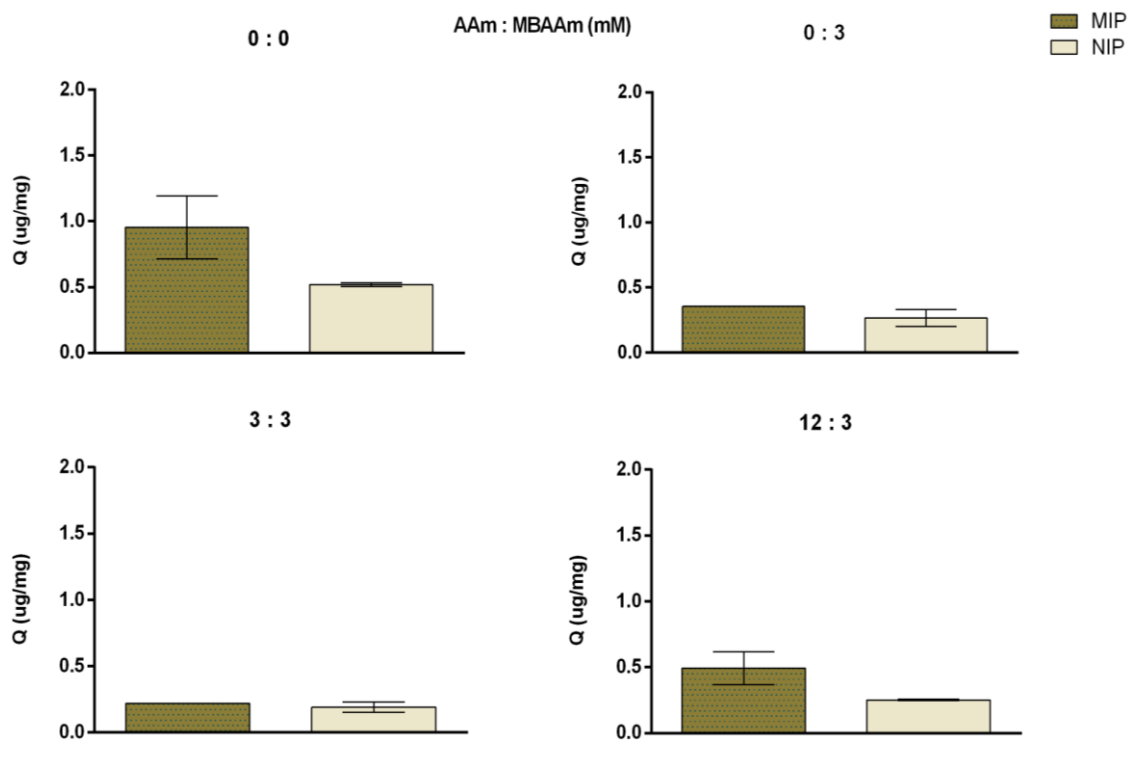

Figure 5.15. Rebinding capacity (amount of BSA adsorbed during rebinding assay) of MIP and NIP discs after 28h incubation in 0.1% BSA solution in 0.9% NaCl. Data represent mean values of n=3 ± SEM.

Table 5.6. Rebinding capacity (Q) and imprinting factor (IF) of MIP and NIP discs after 28h incubation in 0.1% BSA solution in 0.9% NaCl. Data represents mean values of n=3 ± SEM and values correspond to **Figure 5.15**. (* values of n=1)

AAm : MBAAm (mM)		Q (µg/mg)	IF
0 : 0	NIP	0.519 ± 0.013	1.86 ± 0.51
	MIP	0.955 ± 0.239	
0 : 3	NIP	0.267 ± 0.063	1.41 ± 0.34
	MIP	0.355 ± *	
3 : 3	NIP	0.191 ± 0.037	1.19 ± 0.23
	MIP	0.218 ± *	
12 : 3	NIP	0.252 ± 0.007	1.98 ± 0.58
	MIP	0.494 ± 0.125	

Overall, these results pointed out that ALMA modified with only a crosslinker, as MBAAm, was an unsuccessful procedure to define a suitable imprinted cavity for BSA. In turn, the same amount of monomer and crosslinker in the presence of ALMA was also unsuccessful combination, as the difference between MIP and NIP behaviour with 3:3 ratio was minimal. In addition, the 12:3 discs did not display significant swelling, meaning that the imprinted cavities did not suffer much distortion during the water uptake. This also highlights the need for monomer/crosslinkers to achieve good recognition characteristics.

Thus, at this stage it was clear that a higher amount of monomer compared to the cross-linker was necessary, as this would increase the ability of the disc to recognize the imprinted protein. In turn, the imprinting efficiency must be tuned with a lower amount of entrapped protein, as this is an expensive component within the imprinting process. Moreover, the entrapped protein must not contribute to an immunogenic response, or else the overall process becomes ineffective for TE applications.

Chapter 6 - Conclusions and perspectives

In the present work, a molecular imprinting system based on photosensitive methacrylated alginate was developed and characterized. MIP discs were produced using a model protein, BSA, as template. This protein is widely used as the control/blank in many works, due to its prompt availability and low price; in this work it was used to accomplish the optimization of the polymeric system for future studies, with proteins more promising for TE applications.

The role of crosslinkers and monomers upon the imprinting features and the mechanical properties of the polymer discs were successfully studied and the results revealed an increase on the mechanical properties of the crosslinked polymers, as expected. Further studies should comprise the use of other crosslinkers and monomers, aiming to improve the mean pore size of the final hydrogel.

A template removal protocol was also performed, mostly by changing the pH where the discs were incubated. The discs released about 70% of the BSA used in the imprinting stage. In the future, some improvements may be established herein, regarding the time and medium of incubation, as well as the composition of the imprinted material (kind of monomer and cross-linker, along with their ratio).

The rebinding capacity of NIP and MIP discs was further evaluated, leading to better results for discs prepared with monomer and crosslinker (12:3, respectively). As usual in science, this protocol could also be subject to further improvements. One change could be, after the stage of template removal was finished, incubate the discs in 0.9% NaCl solution (pH 4.2) prior to the incubation in the rebinding solution, to adjust the discs to the new pH and improve the protein adsorption.

Overall, it became clear from this work that the presence of monomer and crosslinker, with high ratio of monomer/crosslinker, were fundamental conditions to confer the material the ability to recognize the protein. Other ratios than 12:3 could be further studies as well as other types of monomers and crosslinkers to improve the obtained data, especially to different behaviour between MIP materials and their control (NIP materials). The amount of photoinitiator and the time of UV irradiation could also be further tuned, along with these, to ensure that most of the vinyl-based materials reacted along the formation of the material.

As future perspectives for this work, it may be said that the study presented herein seems promising, opening doors towards the imprinting technology within TE and hydrogels, which is a reasonably recent topic. The ability of protein recognition in a hydrogel composition that meets basic requirements in TE has been proven. Of course, as expressed before, further studies are necessary to improve this work and to meet the current needs for real TE applications.

References

[1] A. Atala, D. J. Irvine, M. Moses, and S. Shaunak, "Wound Healing Versus Regeneration: Role of the Tissue Environment in Regenerative Medicine," *MRS Bull.*, vol. 35, no. 8, pp. 597–606, 2010.

[2] G. S. Schultz and A. Wysocki, "Interactions between extracellular matrix and growth factors in wound healing," *Wound Repair Regen.*, vol. 17, no. 2, pp. 153–162, 2009.

[3] K. S. Midwood, L. V. Williams, and J. E. Schwarzbauer, "Tissue repair and the dynamics of the extracellular matrix," *Int. J. Biochem. Cell Biol.*, vol. 36, pp. 1031–1037, 2004.

[4] M. S. Hu, Z. N. Maan, J.-C. Wu, R. C. Rennert, W. X. Hong, T. S. Lai, A. T. M. Cheung, G. G. Walmsley, M. T. Chung, A. McArdle, M. T. Longaker, and H. P. Lorenz, "Tissue Engineering and Regenerative Repair in Wound Healing," *Ann. Biomed. Eng.*, vol. 42, no. 7, pp. 1494–1507, 2014.

[5] C. Frantz, K. M. Stewart, and V. M. Weaver, "The extracellular matrix at a glance," *J. Cell Sci.*, vol. 123, no. 24, pp. 4195–4200, 2010.

[6] W. J. Li, R. Tuli, C. Okafor, A. Derfoul, K. G. Danielson, D. J. Hall, and R. S. Tuan, "A three-dimensional nanofibrous scaffold for cartilage tissue engineering using human mesenchymal stem cells," *Biomaterials*, vol. 26, no. 6, pp. 599–609, 2005.

[7] A. Wang, Z. Tang, I.-H. Park, Y. Zhu, S. Patel, G. Q. Daley, and S. Li, "Induced pluripotent stem cells for neural tissue engineering," *Biomaterials*, vol. 32, no. 22, pp. 5023–5032, 2011.

[8] G. F. MUSCHLER, C. NAKAMOTO, and L. G. GRIFFITH, "Engineering Principles of Clinical Cell-Based Tissue Engineering," *J. Bone Jt. Surgery-American Vol.*, vol. 86, no. 7, pp. 1541–1558, 2004.

[9] R. Balint, N. J. Cassidy, and S. H. Cartmell, "Electrical Stimulation: A Novel Tool for Tissue Engineering," *Tissue Eng. Part B-Reviews*, vol. 19, no. 1, pp. 48–57, 2013.

[10] C. Sekirnjak, P. Hottowy, A. Sher, W. Dabrowski, A. M. Litke, and E. J. Chichilnisky, "High-Resolution Electrical Stimulation of Primate Retina for Epiretinal Implant Design," *J. Neurosci.*, vol. 28, no. 17, pp. 4446–4456, 2008.

[11] I. Titushkin and M. Cho, "Regulation of cell cytoskeleton and membrane mechanics by electric field: Role of linker proteins," *Biophys. J.*, vol. 96, no. 2, pp. 717–728, 2009.

[12] S. C. Neves, D. B. Gomes, A. Sousa, S. J. Bidarra, P. Petrini, L. Moroni, C. C. Barrias, and P. L. Granja, "Biofunctionalized pectin hydrogels as 3D cellular microenvironments," *J. Mater. Chem. B*, vol. 3, no. 10, pp. 2096–2108, 2015.

[13] D. Ko buk, S. Guimond-Lischer, P. Sajkiewicz, K. Maniura-Weber, and G. Fortunato, "Morphology and surface chemistry of bicomponent scaffolds in terms of mesenchymal stromal cell viability," *J. Bioact. Compat. Polym.*, vol. 31, no. 4, pp. 423–436, 2016.

[14] H. Jarvelainen, A. Sainio, M. Koulu, T. N. Wight, and R. Penttinen, "Extracellular Matrix Molecules: Potential Targets in Pharmacotherapy," *Pharmacol. Rev.*, vol. 61, no. 2, pp. 198–223, 2009.

[15] T. Rozario and D. W. DeSimone, "The extracellular matrix in development and morphogenesis: A dynamic view," *Dev. Biol.*, vol. 341, no. 1, pp. 126–140, 2010.

[16] S. Ricard-Blum, "The Collagen Family," *Cold Spring Harb. Perspect. Biol.*, vol. 3, no. 1, pp. 1–19, 2011.

[17] A. J. Zollinger and M. L. Smith, "Fibronectin , the extracellular glue," *Matrix Biol.*, 2016.

[18] J. Sottile and D. C. Hocking, "Fibronectin Polymerization Regulates the Composition and Stability of Extracellular Matrix Fibrils and Cell-Matrix Adhesions," *Mol. Biol. Cell*, vol. 13, pp. 3546–3559, 2002.

[19] W. P. Daley, S. B. Peters, and M. Larsen, "Extracellular matrix dynamics in development and regenerative medicine," *J. Cell Sci.*, vol. 121, no. 3, pp. 255–264, 2008.

[20] M. Giannandrea and W. C. Parks, "Diverse functions of matrix metalloproteinases during fibrosis," *Dis. Model. Mech.*, vol. 7, no. 2, pp. 193–203, 2014.

[21] A. Walker, J. E. Turnbull, and J. T. Gallagher, "Specific heparan sulfate saccharides mediate the activity of basic fibroblast growth factor," *J. Biol. Chem.*, vol. 269, no. 2, pp. 931–935, 1994.

[22] S. Matsumoto, R. Tanaka, K. Okada, K. Arita, H. Hyakusoku, M. Miyamoto, Y. Tabata, and H. Mizuno, "The Effect of Control-released Basic Fibroblast Growth Factor in Wound Healing: Histological Analyses and Clinical Application.," *Plast. Reconstr. surgery. Glob. open*, vol. 1, no. 6, p. e44, Sep. 2013.

[23] R. a Ignotz and J. Massagué, "Transforming growth factor-beta stimulates the expression of fibronectin and collagen and their incorporation into the extracellular matrix.," *J. Biol. Chem.*, vol. 261, no. 9, pp. 4337–45, 1986.

[24] L. Ma, C. Gao, Z. Mao, J. Zhou, J. Shen, X. Hu, and C. Han, "Collagen/chitosan porous scaffolds with improved biostability for skin tissue engineering," *Biomaterials*, vol. 24, no. 26, pp. 4833–4841, 2003.

[25] A. Barbetta, E. Barigelli, and M. Dentini, "Porous alginate hydrogels: Synthetic methods for tailoring the porous texture," *Biomacromolecules*, vol. 10, no. 8, pp. 2328–2337, 2009.

[26] T. Tokatlian, C. Cam, and T. Segura, "Non-viral DNA delivery from porous hyaluronic acid hydrogels in mice," *Biomaterials*, vol. 35, no. 2, pp. 825–835, 2014.

[27] M. Spoliti, P. Iudicone, R. Leone, A. De Rosa, F. R. Rossetti, and L. Pierelli, "In vitro release and expansion of mesenchymal stem cells by a hyaluronic acid scaffold used in combination with bone marrow.," *Muscles. Ligaments Tendons J.*, vol. 2, no. 4, pp. 289–94, 2012.

[28] M.-H. Ho, P.-Y. Kuo, H.-J. Hsieh, T.-Y. Hsien, L.-T. Hou, J.-Y. Lai, and D.-M. Wang, "Preparation of porous scaffolds by using freeze-extraction and freeze-gelation methods," *Biomaterials*, vol. 25, pp. 129–138, 2004.

[29] Y. Li, P. Fan, X. M. Ding, X. H. Tian, X. S. Feng, H. Yan, X. M. Pan, P. X. Tian, J. Zheng, C. G. Ding, and W. J. Xue, "Polyglycolic acid fibrous scaffold improving endothelial cell coating and vascularization of islet," *Chin. Med. J. (Engl).*, vol. 130, no. 7, pp. 832–839, 2017.

[30] Z. Ma, C. Gao, Y. Gong, and J. Shen, "Cartilage tissue engineering PLLA scaffold with surface immobilized collagen and basic fibroblast growth factor," *Biomaterials*, vol. 26, no. 11, pp. 1253–1259, 2005.

[31] J. Chahla, C. S. Dean, T. R. Cram, D. Civitarese, L. O'Brien, S. G. Moulton, and R. F. LaPrade, "Two-Stage Revision Anterior Cruciate Ligament Reconstruction: Bone Grafting Technique Using an Allograft Bone Matrix," *Arthrosc. Tech.*, vol. 5, no. 1, pp. e189–e195, 2016.

[32] S. Saber-Samandari and S. Saber-Samandari, "Biocompatible nanocomposite scaffolds based on copolymer-grafted chitosan for bone tissue engineering with drug delivery capability," *Mater. Sci. Eng. C*, vol. 75, no. March, pp. 721–732, 2017.

[33] Q. Ul, A. Nawaz, M. Nabavinia, and M. Mujahid, "Enhanced mechanical properties and biocompatibility of novel hydroxyapatite / TOPAS hybrid composite for bone tissue engineering applications," *Mater. Sci. Eng. C*, vol. 75, no. May, pp. 807–815, 2017.

[34] S. L. Sing, S. Wang, S. Agarwala, F. E. Wiria, T. Mai, H. Ha, and W. Y. Yeong, "Fabrication of titanium based biphasic scaffold using selective laser melting and collagen immersion," *Int. J. Bioprinting*, vol. 3, no. 1, pp. 1–7, 2017.

[35] B. P. Chan and K. W. Leong, "Scaffolding in tissue engineering: General approaches and tissue-specific considerations," *Eur. Spine J.*, vol. 17, no. SUPPL. 4, 2008.

[36] F. Dehghani and N. Annabi, "Engineering porous scaffolds using gas-based techniques," *Curr. Opin. Biotechnol.*, vol. 22, pp. 661–666, 2011.

[37] N. Annabi, J. W. Nichol, X. Zhong, C. Ji, S. Koshy, A. Khademhosseini, and F. Dehghani, "Controlling the Porosity and Microarchitecture of Hydrogels for Tissue Engineering," *Tissue Eng. Part B Rev.*, vol. 16, no. 4, pp. 371–383, 2010.

[38] C. Y. Hsieh, S. P. Tsai, M. H. Ho, D. M. Wang, C. E. Liu, C. H. Hsieh, H. C. Tseng, and H. J. Hsieh, "Analysis of freeze-gelation and cross-linking processes for preparing porous chitosan scaffolds," *Carbohydr. Polym.*, vol. 67, no. 1, pp. 124–132, 2007.

[39] F. J. O'Brien, B. A. Harley, I. V. Yannas, and L. Gibson, "Influence of freezing rate on pore structure in freeze-dried collagen-GAG scaffolds," *Biomaterials*, vol. 25, no. 6, pp. 1077–1086, 2004.

[40] A. J. García, "Interfaces to Control Cell-Biomaterial Adhesive Interactions," *Adv Polym Sci*, vol. 203, pp. 171–190, 2006.

[41] M. Tallawi, E. Rosellini, N. Barbani, M. G. Cascone, R. Rai, G. Saint-Pierre, and A. R. Boccaccini, "Strategies for the chemical and biological functionalization of scaffolds for cardiac tissue engineering: a review," *J. R. Soc. Interface*, vol. 12, no. 108, p. 20150254, 2015.

[42] A. Dolatshahi-Pirouz, T. Jensen, D. C. Kraft, M. Foss, P. Kingshott, J. L. Hansen, A. N. Larsen, J. Chevallier, and F. Besenbacher, "Fibronectin adsorption, cell adhesion, and proliferation on nanostructured tantalum surfaces," *ACS Nano*, vol. 4, no. 5, pp. 2874–2882, 2010.

[43] R. H. Schmedlen, K. S. Masters, and J. L. West, "Photocrosslinkable polyvinyl alcohol hydrogels that can be modified with cell adhesion peptides for use in tissue engineering," *Biomaterials*, vol. 23, pp. 4325–4332, 2002.

[44] S. Sambu, X. Xu, H. a Schiffer, Z. F. Cui, and H. Ye, "RGDS-fuctionalized alginates improve the survival rate of encapsulated embryonic stem cells during cryopreservation.," *Cryo Letters*, vol. 32, no. 5, pp. 389–401, 2011.

[45] V. L. Tsang, A. A. Chen, L. M. Cho, K. D. Jadin, R. L. Sah, S. DeLong, J. L. West, and S. N. Bhatia, "Fabrication of 3D hepatic tissues by additive photopatterning of cellular hydrogels," *FASEB J.*, vol. 21, no. 3, pp. 790–801, 2007.

[46] E. Ruoslahti, "RGD AND OTHER RECOGNITION SEQUENCES FOR INTEGRINS," *Annu. Rev. Cell Dev. Biol*, vol. 12, pp. 697–715, 1996.

[47] S. G. Guerreiro, M. J. Oliveira, M. A. Barbosa, R. Soares, and P. L. Granja, "Neonatal human dermal fibroblasts immobilized in RGD-alginate induce angiogenesis," *Cell Transplant.*, vol. 23, no. 8, pp. 945–957, 2014.

[48] M. I. Neves, M. E. Wechsler, M. E. Gomes, R. L. Reis, P. L. Granja, and N. A. Peppas, "Molecularly Imprinted Intelligent Scaffolds for Tissue Engineering Applications," *Tissue Eng. Part B Rev.*, vol. 23, no. 1, pp. 27–43, 2017.

[49] J.-D. Lei and T.-W. Tan, "Enantioselective separation of naproxen and investigation of affinity chromatography model using molecular imprinting," *Biochem. Eng. J.*, vol. 11, pp. 175–179, 2002.

[50] F. T. C. Moreira, A. H. Kamel, J. R. L. Guerreiro, M. Goreti, and F. Sales, "Man-tailored biomimetic sensor of molecularly imprinted materials for the potentiometric measurement of oxytetracycline," *Biosens. Bioelectron.*, vol. 26, pp. 566–574, 2010.

[51] Y. Wang, Z. Zhang, V. Jain, J. Yi, S. Mueller, J. Sokolov, Z. Liu, K. Levon, B. Rigas, and M. H. Rafailovich, "Potentiometric sensors based on surface molecular imprinting: Detection of cancer biomarkers and viruses," *Sensors Actuators, B Chem.*, vol. 146, no. 1, pp. 381–387, 2010.

[52] C.-H. Lu, Y. Zhang, S.-F. Tang, Z.-B. Fang, H.-H. Yang, X. Chen, and G.-N. Chen, "Sensing HIV related protein using epitope imprinted hydrophilic polymer coated quartz crystal microbalance," *Biosens. Bioelectron.*, vol. 31, pp. 439–444, 2011.

[53] A. Rachkov and N. Minoura, "Recognition of oxytocin and oxytocin-related peptides in aqueous media using a molecularly imprinted polymer synthesized by the epitope approach," *J. Chromatogr. A*, vol. 889, pp. 111–118, 2000.

[54] R. Agarwal, V. Singh, P. Jurney, L. Shi, S. V. Sreenivasan, and K. Roy, "Scalable imprinting of shape-specific polymeric nanocarriers using a release layer of switchable water solubility," *ACS Nano*, vol. 6, no. 3, pp. 2524–2531, 2012.

[55] K. Zhao, T. Chen, B. Lin, W. Cui, B. Kan, N. Yang, X. Zhou, X. Zhang, and J. Wei, "Adsorption and recognition of protein molecular imprinted calcium alginate/polyacrylamide hydrogel film with good regeneration performance and high toughness," *React. Funct. Polym.*, vol. 87, no. March, pp. 7–14, 2015.

[56] D. Zhu, Z. Chen, K. Zhao, B. Kan, L. Liu, X. Dong, H. Wang, C. Zhang, X. Leng, and L. Zhang, "Polypropylene non-woven supported fibronectin molecular imprinted calcium alginate / polyacrylamide hydrogel film for cell adhesion," *Chinese Chem. Lett.*, vol. 26, no. 6, pp. 807–810, 2015.

[57] D. A. Spivak and K. J. Shea, "Investigation into the scope and limitations of molecular imprinting with DNA molecules," *Anal. Chim. Acta*, vol. 435, pp. 65–74, 2001.

[58] S. Yu, A. Q. Luo, D. Biswal, J. Z. Hilt, and D. A. Puleo, "Lysozyme-imprinted polymer synthesized using UV free-radical polymerization," *Talanta*, vol. 83, no. 1, pp. 156–161, 2010.

[59] C. L. Bayer, É. P. Herrero, and N. A. Peppas, "Alginate Films as Macromolecular Imprinted Matrices," *J. Biomater. Sci. Polym. Ed.*, vol. 22, no. 11, pp. 1523–1534, 2011.

[60] W. Yang, Q. Zhou, Q. Lin, Q. Wang, X. Fu, Q. Yang, Q. Zhou, Q. Lin, and C. Wang, "Template-Monomer Interaction in Molecular Imprinting: Is the Strongest the Best?," *Open J. Org. Polym. Mater.*, vol. 5, no. 5, pp. 58–68, 2015.

[61] Y. Q. Xia, T. Y. Guo, M. D. Song, B. H. Zhang, and B. L. Zhang, "Hemoglobin recognition by imprinting in semi-interpenetrating polymer network hydrogel based on polyacrylamide and chitosan," *Biomacromolecules*, vol. 6, no. 5, pp. 2601–2606, 2005.

[62] K. Araki, T. Maruyama, N. Kamiya, and M. Goto, "Metal ion-selective membrane prepared by surface molecular imprinting," *J. Chromatogr. B*, vol. 818, pp. 141–145, 2005.

[63] R. Schirhagl, "Bioapplications for molecularly imprinted polymers," *Anal. Chem.*, vol. 86, no. 1, pp. 250–261, 2014.

[64] R. Schirhagl, P. A. Lieberzeit, and F. L. Dickert, "Chemosensors for Viruses Based on Artificial Immunoglobulin Copies," *Adv. Mater.*, vol. 22, no. 18, pp. 2078–2081, 2010.

[65] D. R. Kryscio and N. A. Peppas, "Acta Biomaterialia Critical review and perspective of macromolecularly imprinted polymers," *Acta Biomater.*, vol. 8, no. 2, pp. 461–473, 2012.

[66] Y.-Q. Xia, T.-Y. Guo, H.-L. Zhao, M.-D. Song, B.-H. Zhang, and B.-L. Zhang, "Protein recognition onto silica particles using chitosan as intermedium substrate," *J. Biomed. Mater. Res. Part A*, vol. 90A, no. 2, pp. 326–332, Aug. 2009.

[67] F. Puoci, F. Iemma, G. Cirillo, N. Picci, P. Matricardi, and F. Alhaique, "Molecularly imprinted polymers for 5-fluorouracil release in biological fluids," *Molecules*, vol. 12, no. 4, pp. 805–814, 2007.

[68]   H. Jeon and G. Kim, "Effects of a Cell-Imprinted Poly (dimethylsiloxane) Surface on the Cellular Activities of MG63 Osteoblast-like Cells : Preparation of a Patterned Surface, Surface Characterization, and Bone Mineralization," *Langmuir*, vol. 28, no. 37, pp. 13423–13430, 2012.

[69]   M. E. Byrne, K. Park, and N. A. Peppas, "Molecular imprinting within hydrogels," *Adv. Drug Deliv. Rev.*, vol. 54, no. 1, pp. 149–161, 2002.

[70]   A. W. Chan and R. J. Neufeld, "Modeling the controllable pH-responsive swelling and pore size of networked alginate based biomaterials," *Biomaterials*, vol. 30, no. 30, pp. 6119–6129, 2009.

[71]   C. Lee, J. Shin, J. S. Lee, E. Byun, J. H. Ryu, S. H. Um, D. I. Kim, H. Lee, and S. W. Cho, "Bioinspired, calcium-free alginate hydrogels with tunable physical and mechanical properties and improved biocompatibility," *Biomacromolecules*, vol. 14, no. 6, pp. 2004–2013, 2013.

[72]   M. B. Mellott, K. Searcy, and M. V. Pishko, "Release of protein from highly cross-linked hydrogels of poly(ethylene glycol) diacrylate fabricated by UV polymerization," *Biomaterials*, vol. 22, no. 9, pp. 929–941, 2001.

[73]   M. Ahearne, Y. Yang, A. J. El Haj, K. Y. Then, and K.-K. Liu, "Characterizing the viscoelastic properties of thin hydrogel-based constructs for tissue engineering applications," *J. R. Soc. Interface*, vol. 2, no. 5, pp. 455–463, 2005.

[74]   H. Tai, D. Howard, S. Takae, W. Wang, T. Vermonden, W. E. Hennink, P. S. Stayton, A. S. Hoffman, A. Endruweit, C. Alexander, S. M. Howdle, and K. M. Shakesheff, "Photo-cross-linked hydrogels from thermoresponsive PEGMEMA-PPGMA-EGDMA copolymers containing multiple methacrylate groups: Mechanical property, swelling, protein release, and cytotoxicity," *Biomacromolecules*, vol. 10, no. 10, pp. 2895–2903, 2009.

[75]   M. Leonard, M. R. De Boisseson, P. Hubert, F. Dalençon, and E. Dellacherie, "Hydrophobically modified alginate hydrogels as protein carriers with specific controlled release properties," *J. Control. Release*, vol. 98, no. 3, pp. 395–405, 2004.

[76]   J. Zhao, X. Zhao, B. Guo, and P. X. Ma, "Multifunctional interpenetrating polymer network hydrogels based on methacrylated alginate for the delivery of small molecule drugs and sustained release of protein," *Biomacromolecules*, vol. 15, no. 9, pp. 3246–3252, 2014.

[77]   X. Wang, T. Hao, J. Qu, C. Wang, and H. Chen, "Synthesis of thermal polymerizable alginate-GMA hydrogel for cell encapsulation," *J. Nanomater.*, vol. 2015, 2015.

[78]   Z. Cai, L. A. Luck, D. Punihaole, J. D. Madura, and S. A. Asher, "Photonic crystal protein hydrogel sensor materials enabled by conformationally induced volume phase transition," *Chem. Sci.*, vol. 7, no. 7, pp. 4557–4562, 2016.

[79]   P. Varde, "Crosslinked Hyaluronic Acid Hydrogel Networks Designed as Mechanical Actuators," *Rejuvenation Res.*, no. May, p. 246, 2015.

[80]   M. Ali and M. E. Byrne, "Controlled release of high molecular weight hyaluronic acid from molecularly imprinted hydrogel contact lenses," *Pharm. Res.*, vol. 26, no. 3, pp. 714–726, 2009.

[81]   O. Jeon, K. H. Bouhadir, J. M. Mansour, and E. Alsberg, "Photocrosslinked alginate hydrogels with tunable biodegradation rates and mechanical properties," *Biomaterials*, vol. 30, no. 14, pp. 2724–2734, 2009.

[82]   C. Gao, M. Liu, J. Chen, and X. Zhang, "Preparation and controlled degradation of oxidized sodium alginate hydrogel," *Polym. Degrad. Stab.*, vol. 94, no. 9, pp. 1405–1410, 2009.

[83]   Y. Huang, S. Onyeri, M. Siewe, A. Moshfeghian, and S. V Madihally, "In vitro characterization of chitosan–gelatin scaffolds for tissue engineering," *Biomaterials*, vol. 26, pp. 7616–7627, 2005.

[84]   P. Iyer, K. J. Walker, and S. V. Madihally, "Increased matrix synthesis by fibroblasts with decreased proliferation on synthetic chitosan-gelatin porous structures," *Biotechnol. Bioeng.*, vol. 109, no. 5, pp. 1314–1325, 2012.

[85]   B. D. Fairbanks, M. P. Schwartz, C. N. Bowman, and K. S. Anseth, "Photoinitiated polymerization of PEG-diacrylate with lithium phenyl-2,4,6-trimethylbenzoylphosphinate: polymerization rate and cytocompatibility," *Biomaterials*, vol. 30, no. 35, pp. 6702–6707, 2009.

[86]   M. L. Oyen, "Mechanical characterisation of hydrogel materials," *Int. Mater. Rev.*, vol. 59, no. 1, pp. 44–59, 2014.

[87]   J. M. Zuidema, C. J. Rivet, R. J. Gilbert, and F. A. Morrison, "A protocol for rheological characterization of hydrogels for tissue engineering strategies," *J. Biomed. Mater. Res. - Part B Appl. Biomater.*, vol. 102, no. 5, pp. 1063–1073, 2014.

[88]   A. D. Augst, H. J. Kong, and D. J. Mooney, "Alginate hydrogels as biomaterials," *Macromol. Biosci.*, vol. 6, no. 8, pp. 623–633, 2006.

[89]   J. Sun and H. Tan, "Alginate-based biomaterials for regenerative medicine applications," *Materials (Basel).*, vol. 6, no. 4, pp. 1285–1309, 2013.

[90]   J. Li, Y. Wu, J. He, and Y. Huang, "A new insight to the effect of calcium concentration on gelation process and physical properties of alginate films," *J. Mater. Sci.*, vol. 51, no. 12, pp. 5791–5801, 2016.

[91]   C. K. Kuo and P. X. Ma, "Ionically crosslinked alginate hydrogels as scaffolds for tissue engineering: Part 1. Structure, gelation rate and mechanical properties," *Biomaterials*, vol. 22, no. 6, pp. 511–521, 2001.

[92]   J. A. Rowley, G. Madlambayan, and D. J. Mooney, "Alginate hydrogels as synthetic extracellular matrix materials," *Biomaterials*, vol. 20, no. 1, pp. 45–53, 1999.

[93]   A. D. Rouillard, C. M. Berglund, J. Y. Lee, W. J. Polacheck, Y. Tsui, L. J. Bonassar, and B. J. Kirby, "Methods for Photocrosslinking Alginate Hydrogel Scaffolds with High Cell Viability," *Tissue Eng. Part C Methods*, vol. 17, no. 2, pp. 173–179, 2011.

[94]   M. Mauri, S. Vicini, and M. Castellano, "Gelling process of sodium alginate with bivalent ions rich microsphere: Nature of bivalent ions," in *AIP Conference Proceedings 1736*, 2016, p. 4.

[95]   R. Hernández, J. Sacristán, and C. Mijangos, "Sol/gel transition of aqueous alginate solutions induced by Fe2+ cations," *Macromol. Chem. Phys.*, vol. 211, no. 11, pp. 1254–1260, 2010.

[96]   S. L. Fenn, T. Miao, R. M. Scherrer, and R. A. Oldinski, "Dual-Cross-Linked Methacrylated Alginate Sub-Microspheres for Intracellular Chemotherapeutic Delivery," *ACS Appl. Mater. Interfaces*, vol. 8, no. 28, pp. 17775–17783, 2016.

[97]   K. B. Fonseca, S. J. Bidarra, M. J. Oliveira, P. L. Granja, and C. C. Barrias, "Molecularly designed alginate hydrogels susceptible to local proteolysis as three-dimensional cellular microenvironments," *Acta Biomater.*, vol. 7, no. 4, pp. 1674–1682, 2011.

[98]   K. Zhao, J. Wei, G. Cheng, C. Yang, and L. Chen, "Preparation of bovine serum albumin-imprinted calcium polyacrylate/alginate hybrid microspheres Via Ca2+ crosslinking," *J. Appl. Polym. Sci.*, vol. 113, no. 2, pp. 1133–1140, 2009.

[99]   J. H. Chen, G. P. Li, Q. L. Liu, J. C. Ni, W. B. Wu, and J. M. Lin, "Cr(III) ionic imprinted polyvinyl alcohol/sodium alginate (PVA/SA) porous composite membranes for selective adsorption of Cr(III) ions," *Chem. Eng. J.*, vol. 165, no. 2, pp. 465–473, 2010.

[100]   C. S. Chemicals and C. E. Segment, "Ciba IRGACURE 2959 Ciba IRGACURE 2959," *Coating*, pp. 2–4, 2001.

[101]   N. A. Peppas, J. Z. Hilt, A. Khademhosseini, and R. Langer, "Hydrogels in biology and medicine: From molecular principles to bionanotechnology," *Adv. Mater.*, vol. 18, no. 11,

pp. 1345–1360, 2006.

[102]   I. Donati and S. Paoletti, "Material Properties of Alginates," in *Alginates: Biology and Applications*, 2009, pp. 1–53.

[103]   B. P. Albumin, "Albumin from bovine serum," *SigmaAldrich*, vol. 815, no. 1, pp. 2–5, 1990.

[104]   M. D. Atcc, "Formulation for Dulbecco' s Modified Eagle' s," *Amino Acids*, vol. 2, no. 3, pp. 20108–20108, 2002.

[105]   F. S. Bugti, "Detection of differentially expressed proteins in sera of patients with hepatocellular carcinoma by sodium dodecyl sulphate poly-acrylamide gel electrophoresis (SDS-PAGE)," *Pure Appl. Biol.*, vol. 6, no. 1, 2017.

[106]   M. Uygun, M. U. Kahveci, D. Odaci, S. Timur, and Y. Yagci, "Antibacterial acrylamide hydrogels containing silver nanoparticles by simultaneous photoinduced free radical polymerization and electron transfer processes," *Macromol. Chem. Phys.*, vol. 210, no. 21, pp. 1867–1875, 2009.

Supplementary data
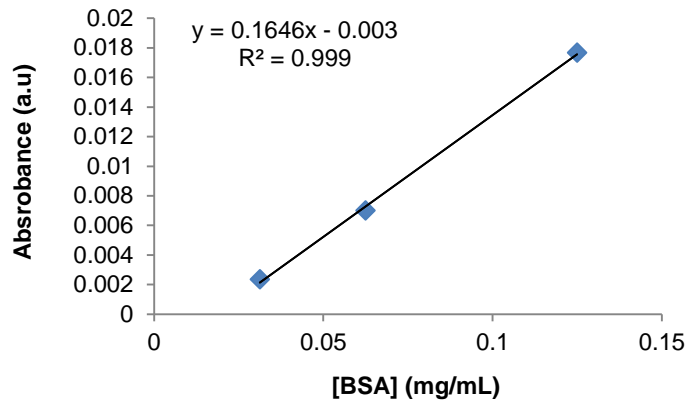
S1. Calibration curve obtained from standard samples (3 readings *per* sample) by DC Protein Assay and reading absorbance at 750nm. The constants *a* and *b* obtained for this calibration curve were 0.1646 and −0.003, respectively.
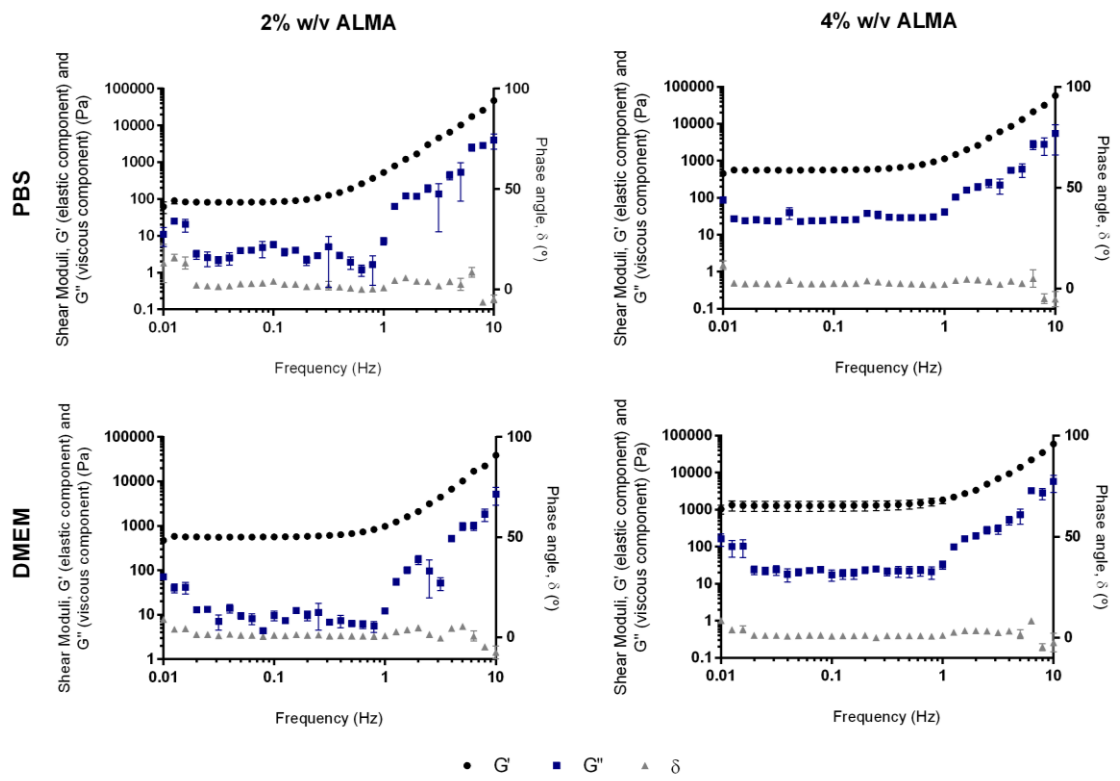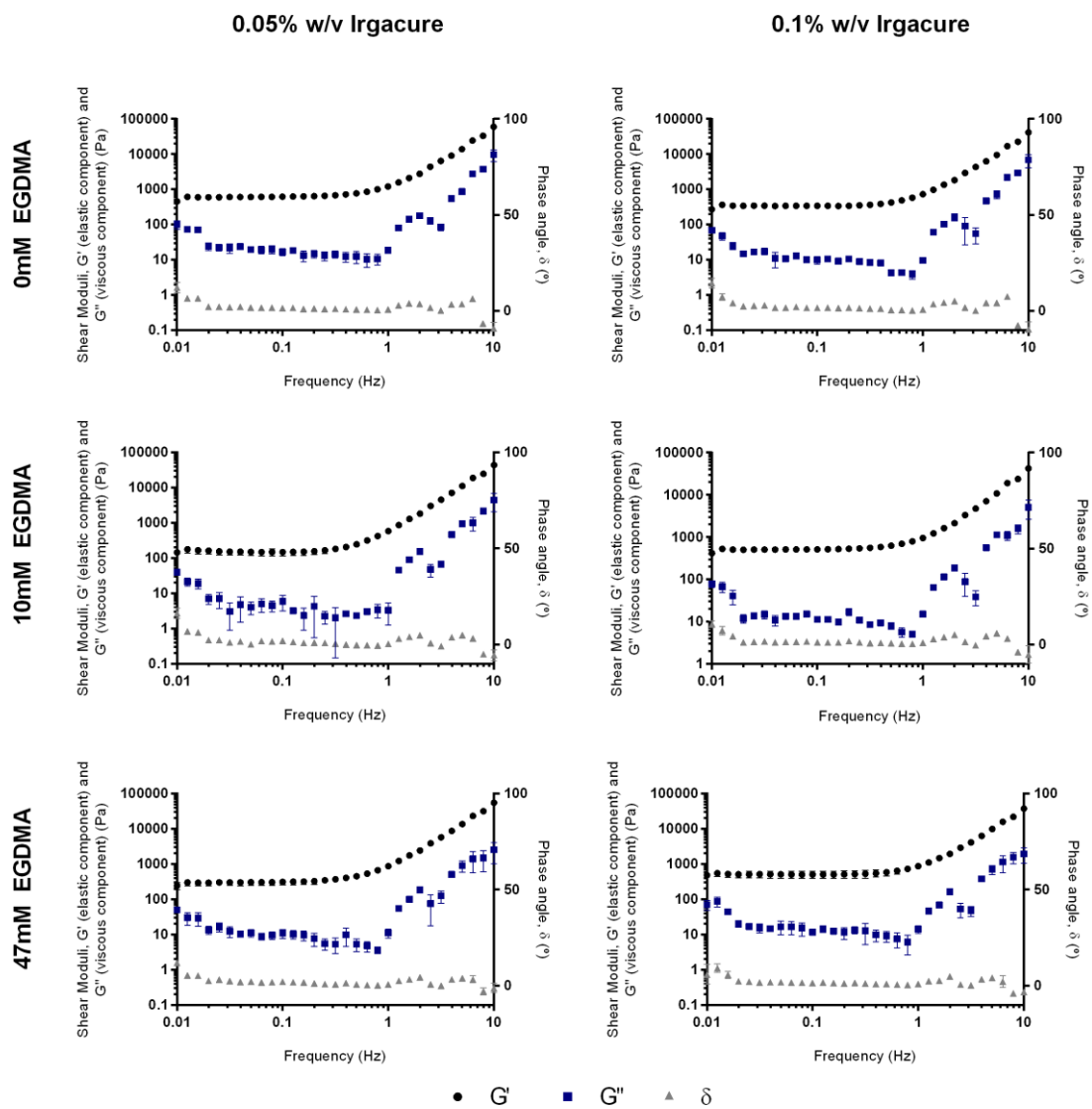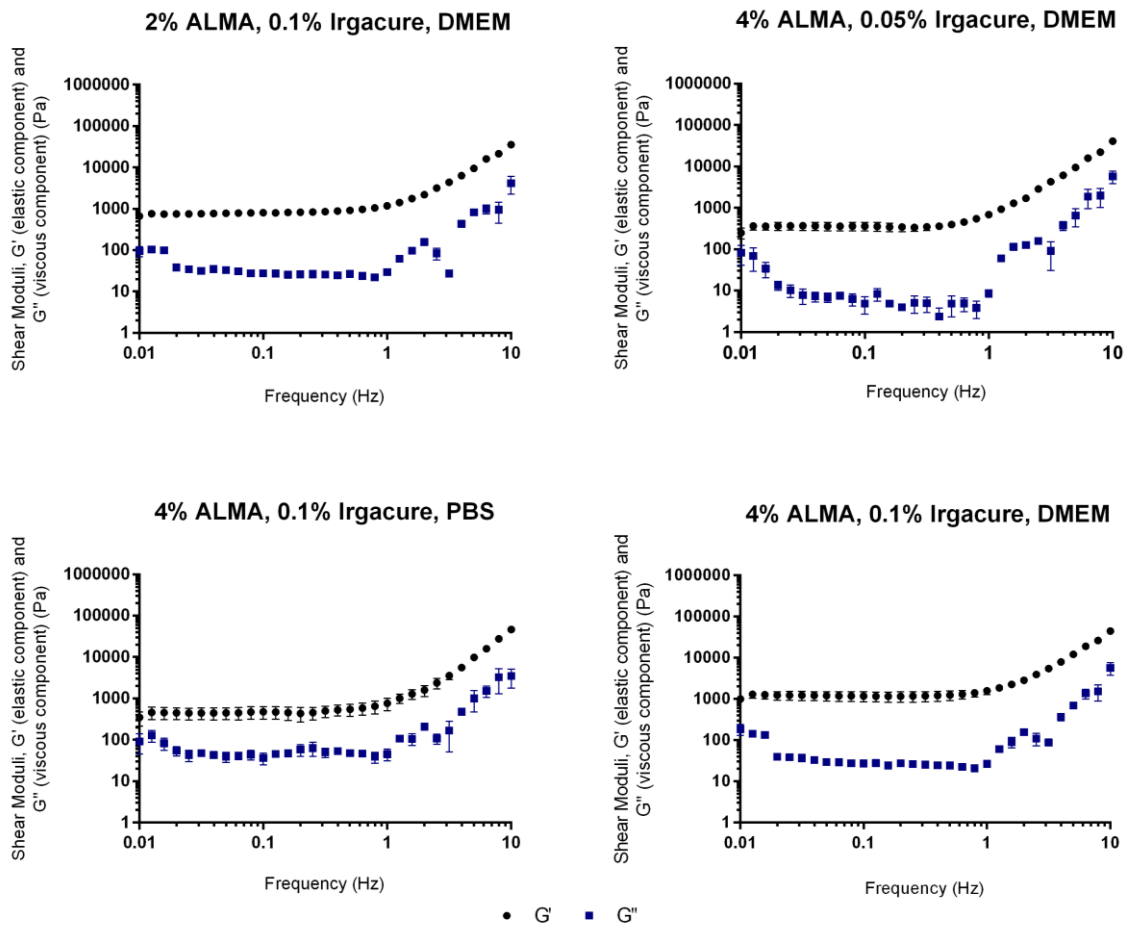
.
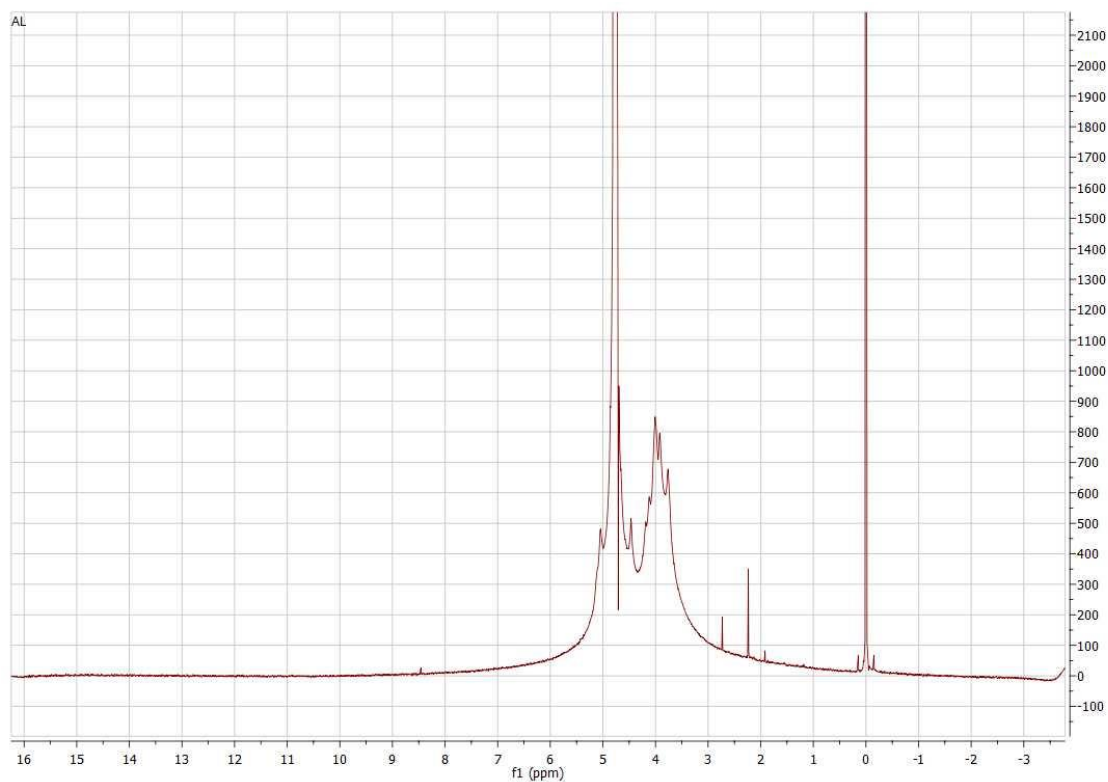
S2. ^{1}H NMR spectra of non-modified alginate (AL).

A
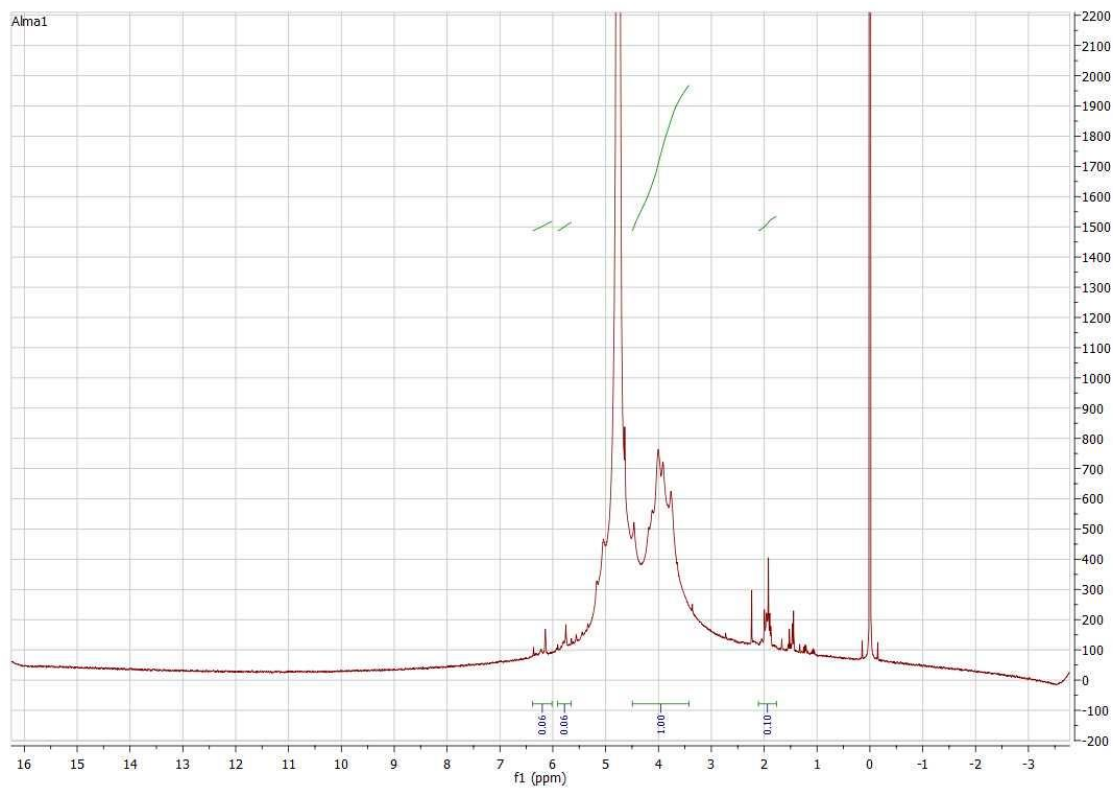
B
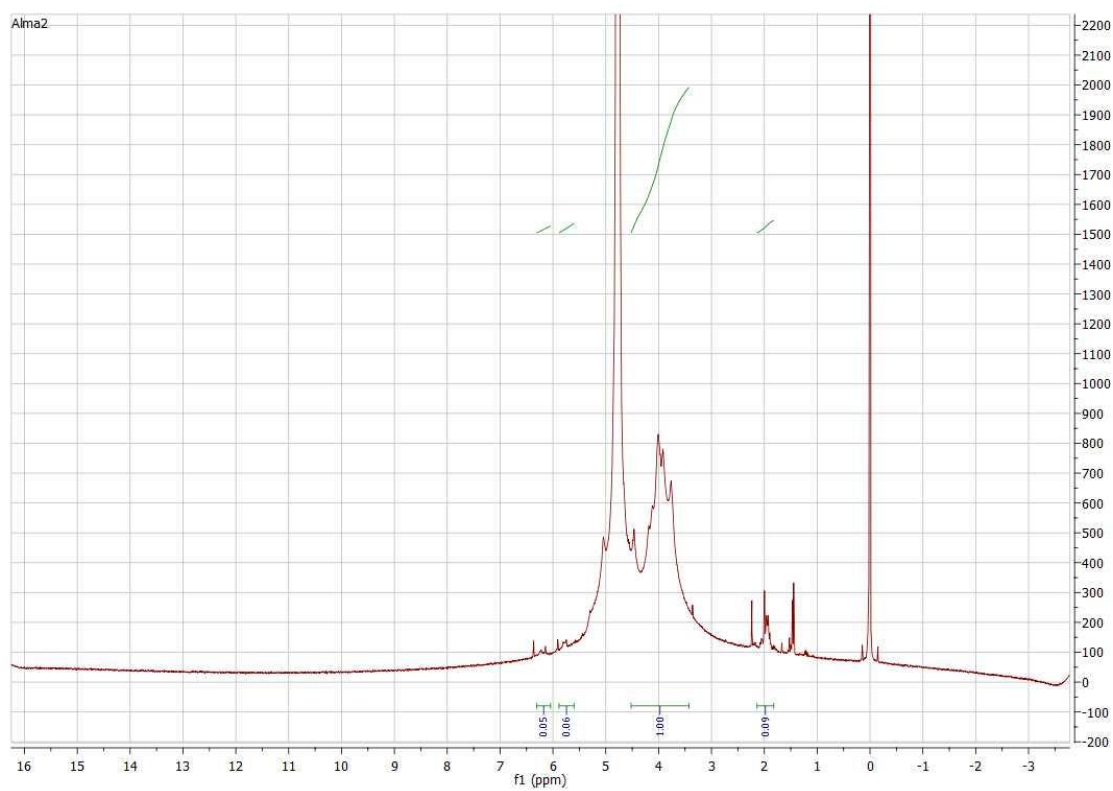
S3. ^{1}H NMR spectra integration of modified alginate (ALMA).

60

S4. Rheological analysis of ALMA NIP discs (2% or 4% w/v ALMA) after 24h incubation in PBS or DMEM.

S5. Rheological analysis of non-crosslinked and crosslinked NIP discs with EGDMA (10mM or 47mM) and 0.05% or 0.1% w/v solution of Irgacure, after 24h incubation in PBS or DMEM.

S6. Rheological analysis of ALMA NIP discs (2% or 4% w/v), produced with 0.05% or 0.1% w/v solution of Irgacure, after 24h incubation in PBS or DMEM.

PBS
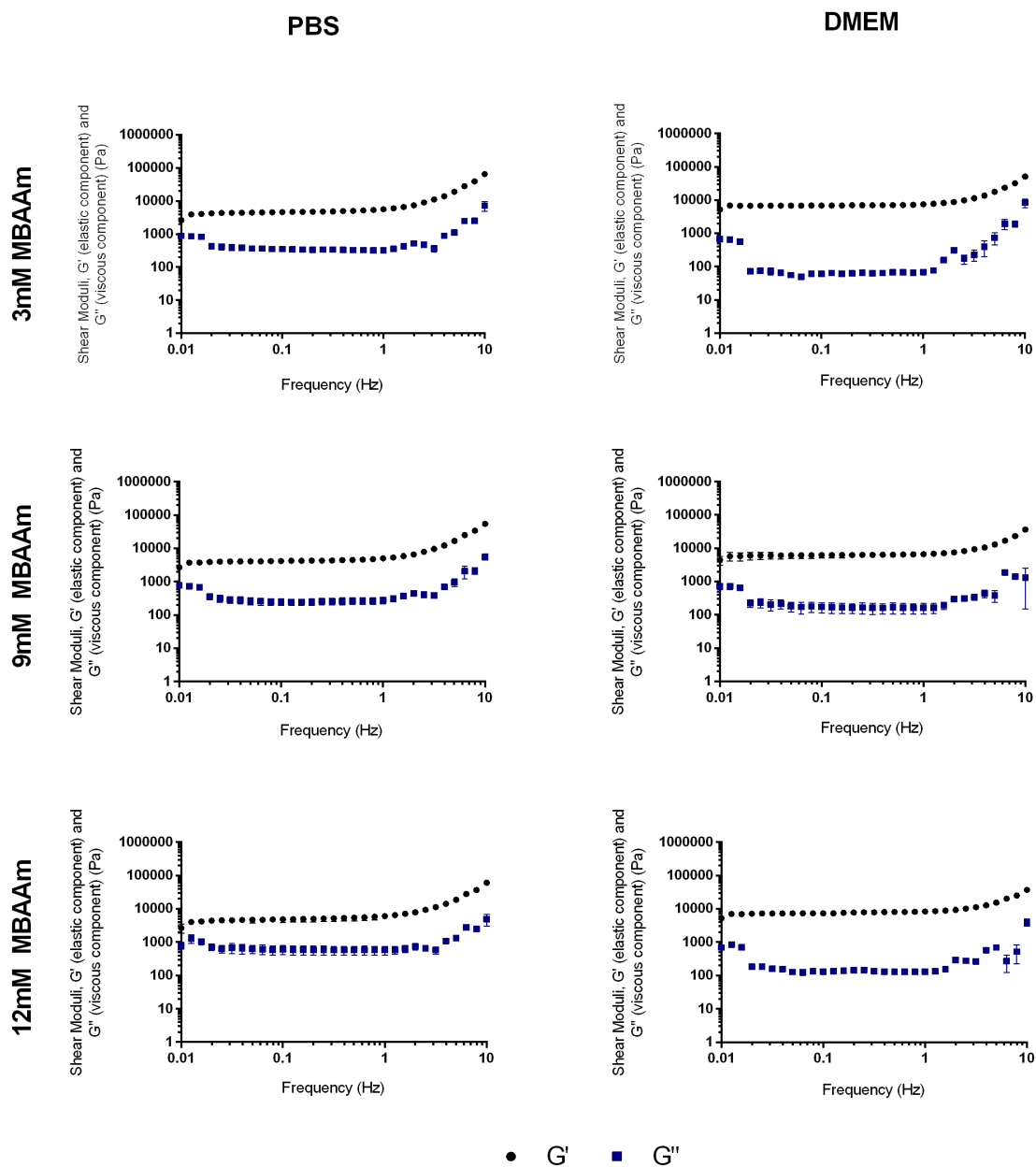
DMEM

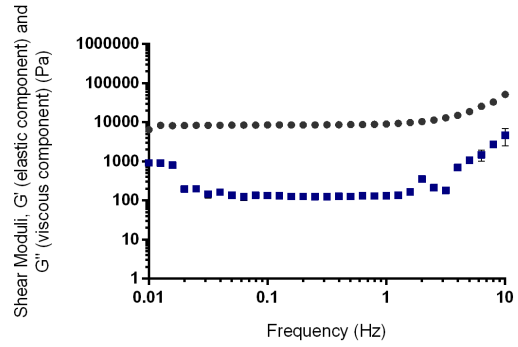**S7.** Rheological analysis of crosslinked NIP discs with MBAAm (3, 9 or 12mM), after 24h incubation in PBS or DMEM.
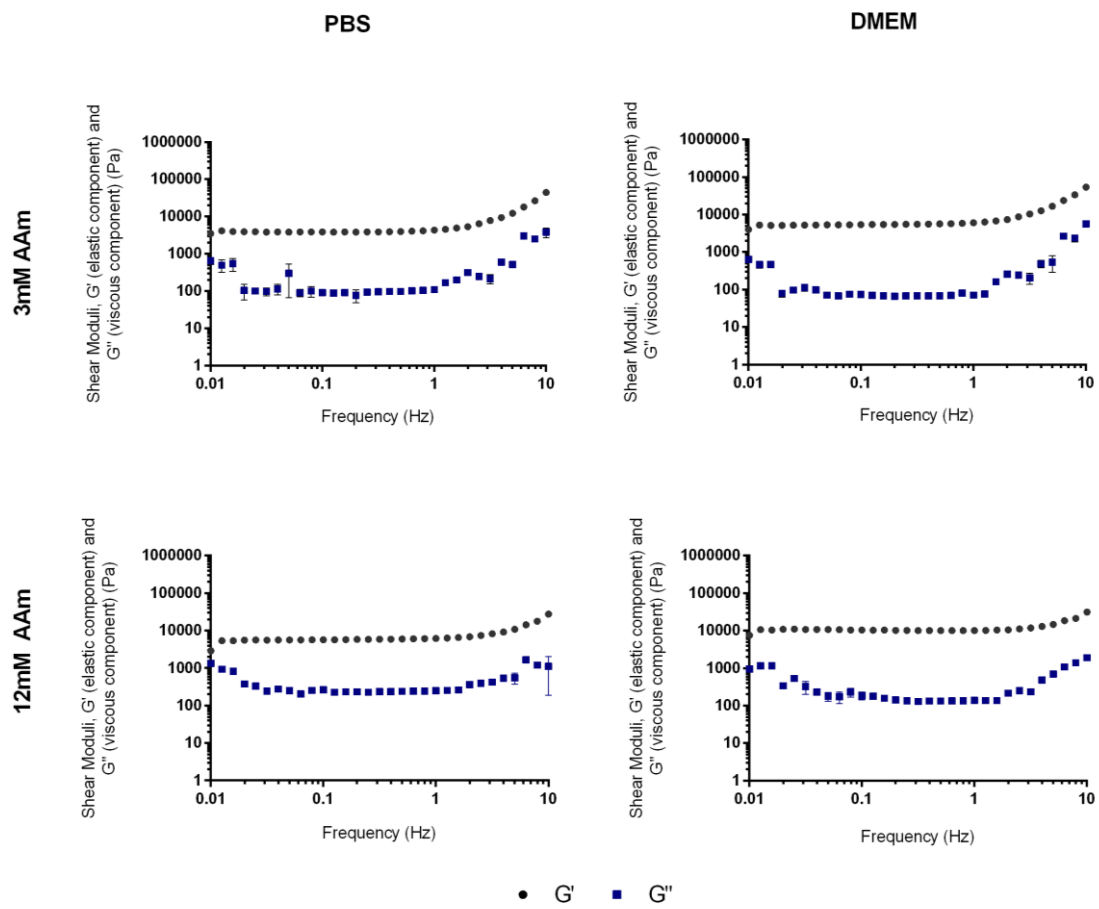
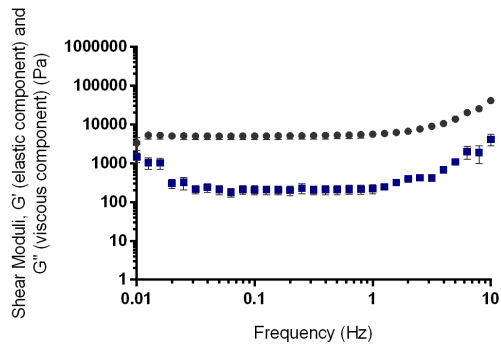**S8.** Rheological analysis of NIP discs produced with AAm (3mM or 12mM), after 24h incubation in PBS or DMEM.
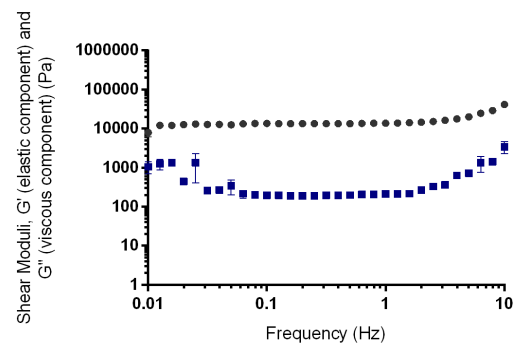
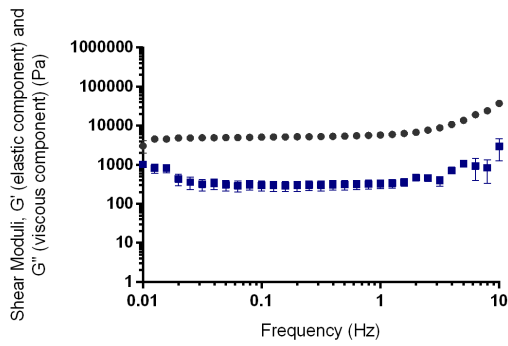**PBS**   **DMEM**

3mM AAm : 3mM MBAAm

12mM AAm : 3mM MBAAm

● G'   ■ G"

S9. Rheological analysis of NIP discs produced with crosslinker MBAAm (3mM) and monomer AAm (3mM or 12mM), after 24h incubation in PBS or DMEM.

66